



Holocene tephrostratigraphic framework and monsoon evolution of East Asia: Key tephra beds for synchronising palaeoclimate records

Xuan-Yu Chen ^{a, b, c, *}, Simon P.E. Blockley ^b, Yi-Gang Xu ^a, Martin A. Menzies ^c

^a State Key Laboratory of Isotope Geochemistry, Guangzhou Institute of Geochemistry, Chinese Academy of Sciences, Guangzhou, 510640, China

^b Department of Geography, Royal Holloway University of London, Egham, Surrey, TW20 0EX, UK

^c Department of Earth Sciences, Royal Holloway University of London, Egham, Surrey, TW20 0EX, UK

ARTICLE INFO

Article history:

Received 2 April 2020

Received in revised form

19 June 2020

Accepted 30 June 2020

Available online 22 July 2020

Keywords:

Tephrochronology

Tephrostratigraphic framework

Cryptotephra

East Asia

Holocene

East Asian summer monsoon

ABSTRACT

In East Asia our understanding of Holocene climate change, forcing mechanisms and propagation, require the precise chronological control of palaeoclimate records to allow robust integration of data sets. The existing chronologies, predominantly based on ¹⁴C method, however, are not sufficient to constrain key questions about abrupt climate shifts that occur within a century in the transitions between states. Widely dispersed tephra layers allow precise dating and synchronisation of sedimentary archives, providing a chronological framework for integrating records, especially where the visible tephra record is complemented by the addition of cryptotephra (non-visible ash). Despite significant tephra studies in this region, however, a comprehensive Holocene tephra framework is not available. To address this issue, we carry out a thorough review on Holocene tephra investigations undertaken in Japan. Using widespread tephra beds we present an integrated tephra framework and suggest the way forward for establishing this as a wider approach for East Asia. The framework is based on twenty-two ash layers that are mainly from Japan, and to a lesser extent China/N Korea, S Korea and Russia. Each tephra is assessed in terms of chronology, geochemistry and distribution. The framework is compared with high resolution palaeoclimate records from East Asia. Using this we demonstrate regional variations in monsoon evolution and more importantly, the potential of tephra isochrons in constraining such variations. Given the scarce identification of tephra layers in those well-resolved palaeoclimate records, we advocate a more systematic employment of the cryptotephra method, which would potentially lead to a significant advance in East Asian tephrochronology and the correlation of palaeoclimate archives in the region.

© 2020 Elsevier Ltd. All rights reserved.

1. Introduction

Tephra is the product of explosive volcanism (Lowe, 2011). Given their synchronous nature, tephra layers have been increasingly used as a key dating and correlation tool for Quaternary studies, providing a framework for synchronising a range of records (e.g., Blockley et al., 2014; Zanchetta et al., 2019). Synchronisation of palaeoclimate records through tephra isochrons allows for the assessment of relative timing and phasing of past changes (e.g., Lane et al., 2013a; Berben et al., 2020). Tephrostratigraphy and Tephrochronology have been based for a number of years on the identification of visible tephra in sedimentary archives. For regions

such as the Mediterranean, tephrochronology has been advanced by using methods such as whole core magnetic susceptibility or quantification of glass shards (e.g. Paterne et al., 1986, 1988; Siani et al., 2004) to identify tephra layers not visible to the naked eye (i.e. cryptotephra). In more recent years this ability to detect cryptotephra has been augmented by the addition of density separation and high-powered microscopy (e.g., Turney, 1998; Blockley et al., 2005). The method has been shown to increase the numbers of tephra that can be detected alongside magnetic and other remote sensing techniques in settings near long term active volcanism (e.g. Bourne et al., 2010; Matthews et al., 2015; Satow et al., 2015), and even detect tephra with extremely small shard concentrations of a few tens of shards per cubic centimetre of sediment, in a range of sedimentary contexts (e.g. Lowe et al., 2012; Blockley et al., 2015; Lane et al., 2015; Wulf et al., 2018). Successful extraction and geochemical characterisation of cryptotephra deposits have now led to the identification of far-travelled tephtras that are able to link

* Corresponding author. State Key Laboratory of Isotope Geochemistry, Guangzhou Institute of Geochemistry, Chinese Academy of Sciences, Guangzhou, 510640, China.

E-mail address: chenxy55@foxmail.com (X.-Y. Chen).

records at hemispheric scale (e.g., Lane et al., 2013b; Jensen et al., 2014; Sun et al., 2014; Bourne et al., 2016; Mackay et al., 2016; van der Bilt et al., 2017; Cook et al., 2018; Smith et al., 2018). However, before records can be confidently correlated using tephra layers, it is of paramount importance to establish a comprehensive regional tephra framework (e.g., Lowe et al., 2008; Zanchetta et al., 2011; Abbott and Davies, 2012; Davies et al., 2012, 2014; Blockley et al., 2014; Bourne et al., 2015; Ikehara, 2015; Lowe et al., 2015; Davies et al., 2016; Nakamura, 2016; Ponomareva et al., 2017; Abbott et al., 2018; Timms et al., 2019).

East Asia possesses significant potential in establishing important tephra frameworks owing to the intensive explosive nature of volcanic activity in this region (see Machida and Arai, 2003). Over the past decades, intensive tephra studies have provided a comprehensive picture for East Asian, but predominantly Japanese, volcanism and allowed the construction of numerous detailed tephrostratigraphies in and around the Sea of Japan area (e.g., Machida and Arai, 1983; Arai et al., 1986; Furuta et al., 1986; Machida, 1999; Aoki and Arai, 2000; Park et al., 2003; Nagahashi et al., 2004; Furukawa and Nanayama, 2006; Aoki et al., 2008; Takemura et al., 2010; Okuno et al., 2011; Smith et al., 2013; Moriwaki et al., 2016; Nakamura, 2016; Razzhigaeva et al., 2016; Sun et al., 2017; Ikehara et al., 2017; Tsuji et al., 2018; Obrochta et al., 2018; Albert et al., 2018, 2019; Pan et al., 2020). However, the reported tephrostratigraphies vary in localities and timeframes, and there is no systematic evaluation of Holocene tephras from a distal viewpoint, to aid the selection of markers that are most useful for correlation purposes. More importantly, previous studies have focused predominantly on visible layers, whereas results from recent studies using cryptotephra extraction techniques (e.g., Sun et al., 2014, 2015; Chen et al., 2016, 2019; McLean et al., 2018, 2020) have demonstrated the necessity to update the available information. For example, the B–Tm tephra from Changbaishan (China/N Korea), which is a visible layer in Japan (Machida and Arai, 2003), has now been identified in Greenland ice-cores as a cryptotephra layer ca. 9000 km from the vent (Sun et al., 2014). A tephra of Kamchatkan provenance has been reported as a cryptotephra horizon in northern Japan, illustrating for the first time a Russian tephra interlinked with Japanese eruptions (Chen et al., 2019). In addition, Holocene ashes from the same volcanic centre in the region can have very similar glass chemistry (e.g., Shiihara et al., 2011; Nakamura, 2016), whose robust correlations require multiple lines of evidence (i.e., geochemical, chronological and stratigraphic evidence etc). As a consequence, an exercise compiling all available information on the most widespread tephras to establish a comprehensive tephrostratigraphic framework is urgently needed, which helps circumvent potential tephra mis-correlation.

Apart from being a volcanically active region, East Asia is also a unique geographical area whose environmental changes are primarily controlled by the East Asian monsoon (EAM) (An, 2000). In this densely populated area, monsoon variability directly impacts a population of over 1.6 billion people (Lu et al., 2013). Nevertheless, a wide range of temporal and spatial patterns of Holocene monsoon evolution have been proposed (e.g., An et al., 2000; Xiao et al., 2004; Zhou et al., 2005; Wang et al., 2005; Dykoski et al., 2005; Shen et al., 2005; Wang et al., 2007; Wu et al., 2012; Lu et al., 2013; Chen et al., 2015; Liu et al., 2015; Stebich et al., 2015; Zhou et al., 2016; Wang et al., 2016; Wen et al., 2017; Zheng et al., 2018; Liu et al., 2020). Regarding the timing and forcing mechanism of East Asian summer monsoon (EASM) variability, two major but conflicting views underpin our current understanding of Holocene climate change. The first interpretation, mainly based on Chinese speleothem records, suggests that the EASM maximum occurred in early Holocene, and that the monsoon intensity responds directly to orbital time scale external forcing (i.e., solar insolation) without a

phase lag (e.g., Wang et al., 2005; Dykoski et al., 2005). The competing view, derived from Chinese lacustrine and loess deposits, however holds that the Holocene Optimum (HO) in the monsoonal region did not commence until the mid-Holocene, which reflects an additional component derived from internal feedback mechanisms (e.g., changes in ice volume and thermohaline circulation) in monsoon evolution (e.g., Xiao et al., 2004; Lu et al., 2013; Chen et al., 2015; Liu et al., 2015; Wen et al., 2017). In addition, syntheses of climate proxy records from lakes and peats in China suggest a time-transgressive onset of the HO in the EAM region, but different studies have come to completely contradictory conclusions. An et al. (2000) proposed a continuously southward retreat of the summer monsoon from ca. 9 ka BP, and that the HO appeared earlier in the north and later in the south. In contrast, Zhou et al. (2016) described a pattern of a gradual northward expansion of the summer monsoon during the Holocene, and that the HO occurred earlier in the south and later in the north. These significant controversies are attributable to chronological uncertainties and ambiguities in interpreting climate proxies obtained from different sedimentary archives (Chen et al., 2015; Wen et al., 2017). Most importantly, high-resolution studies have shown that high-frequency climatic changes, such as centennial-scale changes of monsoon intensity, widely appeared in Holocene records across the EAM region (e.g., Chen et al., 2015; Wang et al., 2016; Park et al., 2019; Liu et al., 2020). Nevertheless, existing chronologies are not sufficient, with centennial-scale errors in many ¹⁴C based chronologies, to constrain the relative timing and phasing of such rapid changes, which are crucial for understanding the monsoon dynamics. As a consequence, the characterisation of rapid monsoon changes and the study of EAM dynamics require palaeoclimate records with more precise chronological control and more robust synchronisation method. The presence of time-parallel tephra beds in various sedimentary archives provides an additional and independent tool for precise dating and synchronisation of records in this climatically significant region.

In this contribution, we undertake a thorough review to select the key tephra markers for East Asia, which are found mostly, so far, in the Japanese Islands. We collate the key information (i.e., chronological, stratigraphic, geochemical and dispersal data) for these tephra beds, which are used to form an integrated tephra framework. The integration represents an attempt to bring together and summarise a comprehensive and up-to-date Holocene tephra framework for the region, and to suggest the way forward for establishing this as a wider framework for the entirety of East Asia. The presented framework, with twenty-two tephra layers is then compared with a compilation of high resolution palaeoclimate records from the region to explore the potential of tephra isochrons in constraining rapid climate shifts. We conclude by providing perspectives for future tephrochronological studies in East Asia.

2. Holocene tephrostratigraphic framework for East Asia

Ideally, the most comprehensive tephra frameworks include tephra findings in both proximal and distal sites, with each tephra layer assessed in detail regarding their volcanic stratigraphy, known distribution (including the main dispersal axis, furthest known dispersal, thickness at the identified location etc), mineral assemblage, glass morphology and chemistry, as well as eruptive age (e.g., Zanchetta et al., 2011). Among all this information, robust geochemical signatures and well-constrained eruptive ages, along with detailed stratigraphic information are the primary data for tephra correlation, especially in distal realms where eruptive details are generally missing (Abbott et al., 2018).

This proposed Holocene tephra framework contains twenty-two ash layers with sixteen originating from Japan, three from South

Korea, two from China/N Korea and one from Russia. While these tephra are, so far, predominantly found in the Japanese Islands, the much wider dispersal of some ashes demonstrates the potential of this outlined framework to be developed in the future. For detailed information of tephra name, provenance, current best age, dispersal axis, most distant distribution and data sources see Table 1. The related volcanic centres are shown in Fig. 1. Summarised information of glass chemistry of these tephra markers is listed in Table 2.

As previously outlined by Chen et al. (2019), Holocene tephra from different regions in NE Asia generally possess distinguishable geochemical signatures. Specifically, the Japanese tephra within the framework predominantly exhibit rhyolitic compositions, with only two ashes containing unambiguous dacitic to andesitic analyses (Ta-d and Ma-f ~ j; Fig. 2a and b). These Japanese tephra are classified as low-K to medium-K series (Fig. 2c). Importantly, the tephra from different volcanic centres in Japan can be clearly distinguished on the K-classification diagram (Fig. 2d). In addition, ashes from volcanoes in central and SW Japan (e.g., Kawagodaira, Sanbe and Kikai; Fig. 1) have apparently higher K₂O contents compared to those from volcanoes in northern Japan (e.g., Tarumai, Komagatake, Towada, Usu and Mashu; Fig. 2d). The South Korean ashes within the framework (U-2, U-3 and U-Ok) are from Ulleungdo volcano (Fig. 1). Glasses of these tephra compositionally straddle the phonolitic and trachytic boundary, and belong to the high-K shoshonite series (Fig. 2a, c). They are very distinctive among all East Asian tephra owing to the extremely elevated total alkaline contents (ca. 12–15 wt%; Fig. 2a). The Chinese/N Korean tephra (B–Tm and B-Sg-08) from Changbaishan volcano have distinctive high-K trachytic to rhyolitic compositions, and thus can

be distinguished from the Ulleungdo ashes (Fig. 2a, c). The only Russian ash within the framework is the SH#12 from Shiveluch volcano (Fig. 1). Glass composition of the tephra plots into the medium-K rhyolitic field, the same as the predominant Japanese tephra (Fig. 2a, c), but can be distinguished from the latter easily, as it is more enriched in K₂O and depleted in CaO (Fig. 2c and Table 2).

In summary, tephra within the framework from different volcanic centres across East Asia possess distinguishable major element glass chemistries (Fig. 2c and d). However, in some cases, separation of ashes erupted from the same volcano requires additional chronological and/or stratigraphic information, which will be discussed in detail in the following sections. It is worth noting that a sufficient database of single grain trace element analyses also needs to be developed in this region for further discrimination purpose, though in some cases trace elements alone are not able to add further discrimination between the products of some volcanic centres (e.g., Tomlinson et al., 2012; Lane et al., 2012).

2.1. Tephra isochrons in early holocene (11.7–8.2 ka BP)

Three tephra fall within the early Holocene period in the framework (using the formal subdivision of the Holocene Epoch from Walker et al. (2019)). They are the Ulleungdo U-Ok/U-4, U-3 tephra and Hokkaido Ta-d tephra (Table 1).

The U-Ok tephra represents the largest known Plinian eruption from the Ulleungdo volcano in the Sea of Japan (Fig. 1). It was dispersed towards the ESE and has been identified in a number of marine cores and archives on the islands of Japan (Machida and Arai, 1983; Machida et al., 1984; Takemura et al., 2010; Smith

Table 1

Summary table of provenance, age and distribution information for the twenty-two tephra layers within the proposed Holocene tephrostratigraphic framework.

Tephra	Source volcano (Country)	Current best age estimate (2σ)	Dispersal axis	Furthest known dispersal	Most distant location	Thickness at the location
Ko-a	Komagatake (J)	1929 CE ¹	ESE	V, 500 km	Kunashir Island ⁷	4 cm
Ko-c1	Komagatake (J)	1856 CE ¹	ENE	V, 550 km	Kunashir Island ⁷	1 cm
Ta-a	Tarumai (J)	1739 CE ²	ENE	V, 600 km	Iturup Island ⁷	1 cm
Ko-c2	Komagatake (J)	1694 CE ¹	ENE	V, 550 km	Kunashir Island/Shikotan Island ⁷	<2 cm
Ta-b	Tarumai (J)	1667 CE ²	E	V, 600 km	Iturup Island ⁷	0.5 cm
Us-b	Usu (J)	1663 CE ³	E	V, 400 km	North Pacific ¹⁷	<1 cm
Ko-d	Komagatake (J)	1640 CE ¹	NW	V, 120 km	Okushiri Island ^{17,18}	<10 cm
Ma-b	Mashu (J)	960–992 CE ⁴	ENE	C, 1150 km	Central Honshu (Lake Suigetsu) ⁴	0 cm
B–Tm	Changbaishan (C/N)	946 CE ⁵	E	C, 9000 km	Greenland ¹⁹	0 cm
SH#12	Shiveluch (R)	1374–1295 cal BP ⁶	SE	C, 1900 km	Rebun Island (Lake Kushu) ⁶	0 cm
Ta-c	Tarumai (J)	2800–2500 cal BP ² /2500–2300 cal BP ⁷	E	V, 450 km	Shikotan Islands ⁷	<8 cm
KGP	Kawagodaira (J)	3160–3137 cal BP ⁸	W	C, 300 km	Central Honshu (Lake Suigetsu) ⁴	0 cm
SOh	Sanbe (J)	4068–4004 cal BP ⁹	ENE	C, 320 km	Central Honshu (Lake Biwa) ¹⁰	0 cm
U-2	Ulleungdo (S)	5681–5619 cal BP ⁴	SE	C, 500 km	Central Honshu (Lake Suigetsu) ⁴	0 cm
To-Cu	Towada (J)	6313–6180 cal BP ¹¹ /5986–5899 cal BP ⁴	SE	C, 700 km	Central Honshu (Lake Suigetsu) ⁴	0 cm
Ko-g	Komagatake (J)	6686–6520 cal BP ¹²	ENE	V, 450 km	Kunashir Island ⁷	1 cm
K-Ah	Kikai (J)	7303–7165 cal BP ¹³	E	V, 1300 km	Central Honshu ²⁰	<10 cm
Ma-f ~ j	Mashu (J)	7670–7480 cal BP ¹⁴	ESE	C, 350 km	Rebun Island (Lake Kushu) ⁶	0 cm
B-Sg-08	Changbaishan (C/N)	8166–8099 cal BP ⁴	N/A	C, 1000 km	Central Honshu (Lake Suigetsu) ⁴	0 cm
U-3	Ulleungdo (S)	8440–8360 cal BP ¹⁵	SE	V, 500 km	Central Honshu (Lake Biwa) ^{21,22}	2.5 cm
Ta-d	Tarumai (J)	9700–9000 cal BP ²	E	V, 200 km	Southern Hokkaido ^{17,18}	10 cm
U-Ok	Ulleungdo (S)	10,255–10177 cal BP ¹⁶	ESE	V, 500 km	Central Honshu (Lake Biwa) ¹⁰	4 cm

Abbreviations: Country: J-Japan, C/N-China/N Korea, S–S Korea, R-Russia; Dispersal: V-visible layer, C-cryptotephra horizon.

References: 1. Katsui and Komuro (1984); 2. Nakamura (2016) and references therein; 3. Ōba et al. (1983); 4. McLean et al. (2018); 5. Oppenheimer et al. (2017); 6. Chen et al. (2019); 7. Razzhigaeva et al. (2016); 8. Tani et al. (2013); 9. Albert et al. (2018); 10. Takemura et al. (2010); 11. Inoue et al. (2011); 12. Chen (2019); 13. Smith et al. (2013); 14. Yamamoto et al. (2010); 15. Im et al. (2012); 16. Smith et al. (2011); 17. Furukawa and Nanayama (2006) and references therein; 18. Machida and Arai (2003) and references therein; 19. Sun et al. (2014); 20. Machida and Arai (1978); 21. Shiihara et al. (2011); 22. Nagahashi et al. (2004).

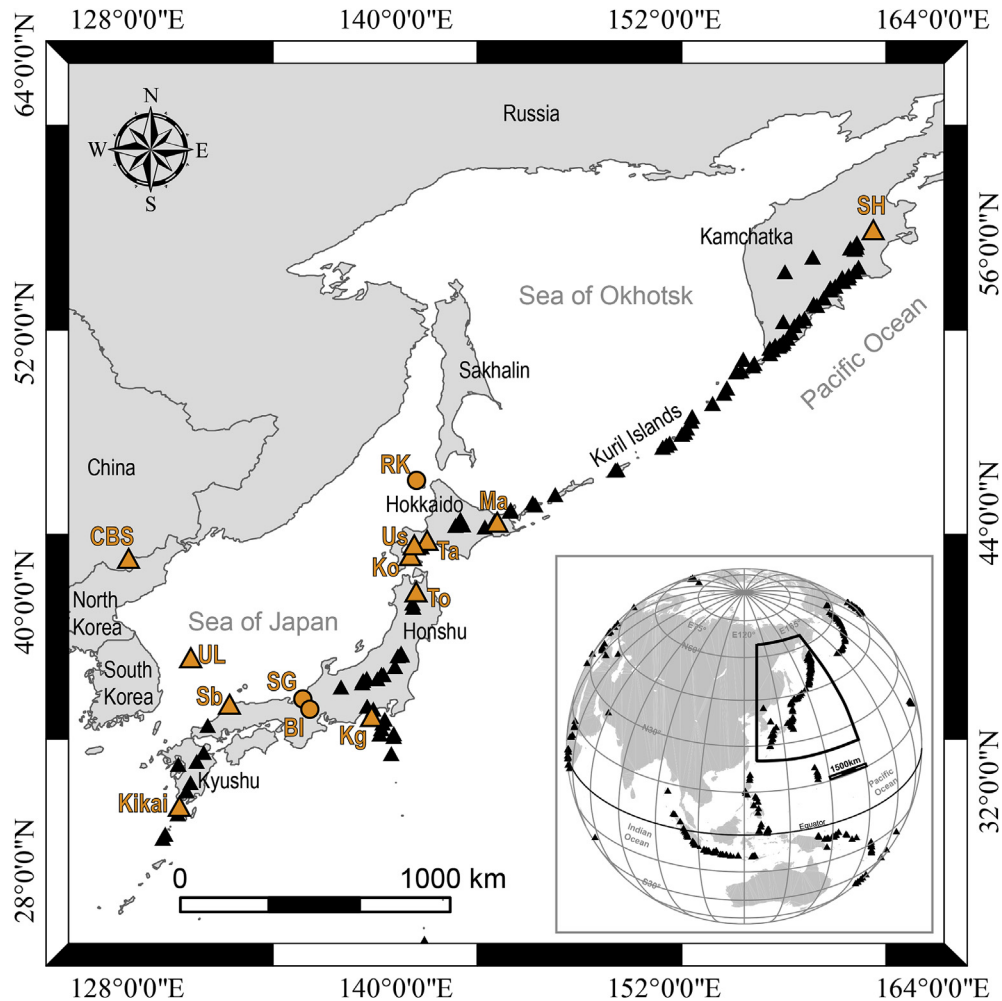


Fig. 1. Map of NE Asia showing volcanoes (triangle) and lacustrine archives for tephra study (circle), with those mentioned in the text highlighted in orange. Abbreviations: Russia: SH-Shiveluch; China/N Korea: CBS-Changbaishan; S Korea: UL-Ulleungdo; Japan: Ma-Mashu, Ta-Tarumai, Us-Usu, Ko-Komagatake, To-Towada, Kg-Kawagodaira, Sb-Sanbe, RK-Lake Kusu (Rebun Island), SG-Lake Suigetsu, BI-Lake Biwa. Kikai is a caldera in southern Kyushu. (For interpretation of the references to colour in this figure legend, the reader is referred to the Web version of this article.)

et al., 2011). Detailed chronological and stratigraphic studies reveal that this tephra can be correlated to the proximal U-4 unit on Ulleungdo Island (Okuno et al., 2010; Shiihara et al., 2011). Glass compositions of the tephra are very homogeneous (ca. 60.5–62.0 wt% SiO₂) (Smith et al., 2011; Shiihara et al., 2011), and are classified as high-K (ca. 6.6–7.5 wt% K₂O) phonolitic to trachytic (Fig. 2a, c). In Lake Suigetsu in central Japan (Fig. 1), a visible ash layer (SG06-1288) has been correlated to the eruption based on glass chemistry (Fig. 3a) and independent chronology (Smith et al., 2011). The Suigetsu SG06 chronology currently provides the best age estimate for the tephra (10,255–10177 cal yr BP (2σ); Smith et al., 2011). This distal age is slightly younger than the proximal ages derived from radiocarbon dating (Okuno et al., 2010) but is supported by a high-resolution proximal Ar–Ar age (Smith et al., 2011). The known distribution of the tephra is based on tracing macroscopic ash layers, which suggest a dispersal area between the volcano and central Honshu (Fig. 4) (Machida and Arai, 1983; Machida et al., 1984; Machida, 1999).

The Ta-d tephra is one of the major tephra markers for northern Japan during the early Holocene (Nakamura, 2016). Emanating from the Tarumai volcano in SW Hokkaido (Fig. 1), the tephra was dispersed mainly toward the east and identified as visible layers ca. 200 km away from the volcano (Fig. 5i) (Machida and Arai, 2003;

Furukawa and Nanayama, 2006). Given its thickness (ca. 10 cm) at the identification locality, and that there is no information regarding its further distribution, it is presumable that the ash should have a much large distribution than that is currently defined. Glasses of the tephra are very distinctive in compositions among all ashes within the framework, and they are low-K (ca. 0.7–1.1 wt% K₂O) andesitic to dacitic (ca. 62.3–65.2 wt% SiO₂; Fig. 2) (Nakamura, 2016). The age of this tephra remains poorly constrained. Based on the calibration of reported radiocarbon dates, Nakamura (2016) calculated an age of 9700–9000 cal yr BP (2σ) for this tephra. Nevertheless, the timing of this tephra, from a climatostratigraphic viewpoint, is very interesting (see discussion). Given that geochemically distinct tephra layer can still serve as correlation tool even when its age is poorly constrained or unknown (Lowe, 2011), future identification of this marker in disparate archives will enable precise test of the synchronicity of climate events across East Asia. It is also worth noting that precise eruptive age of this tephra layer is urgently needed.

The U-3 tephra from Ulleungdo volcano has a more limited known distribution compared to the U-Oki tephra (Fig. 4), as the former has been identified in only a few sequences. Dispersed towards the SE, the marker exists as a cryptotephra horizon in a marine core in southeast Sea of Japan (Domitsu et al., 2002;

Table 2

Summary information of glass chemistry for the twenty-two tephra layers within the proposed Holocene tephrostratigraphic framework. For full dataset see supplementary material.

Tephra	TAS classification	K classification	Compositional range of dominant population (wt%)			SiO ₂ (Avg.,1σ)	TiO ₂ (Avg.,1σ)	Al ₂ O ₃ (Avg.,1σ)	FeO _t (Avg.,1σ)	MnO (Avg.,1σ)	MgO (Avg.,1σ)	CaO (Avg.,1σ)	Na ₂ O (Avg.,1σ)	K ₂ O (Avg.,1σ)	P ₂ O ₅ (Avg.,1σ)	Cl (Avg.,1σ)	n	EPMA data source ref
			SiO ₂	K ₂ O	CaO													
Ko-a	Rhyolitic	Medium-K	76.3	1.8	1.9	77.03	0.47	12.37	2.18	0.13	0.51	2.07	3.32	1.92			10	1*, 2
			-77.5	-2.0	-2.3	0.44	0.07	0.18	0.21	0.08	0.08	0.15	0.11	0.05				
Ko-c1	Rhyolitic	Medium-K	76.2	1.8	2.0	76.44	0.45	12.75	2.21	0.10	0.55	2.30	3.35	1.85			15	1*, 2
			-77.1	-2.0	-2.5	1.24	0.08	0.86	0.20	0.07	0.11	0.45	0.15	0.11				
Ta-a	Rhyolitic	Medium-K	75.3	2.2	1.7	75.80	0.42	13.12	2.22	0.06	0.47	2.32	3.32	2.26			11	1*, 2
			-77.2	-2.4	-2.5	1.91	0.06	1.15	0.31	0.06	0.08	0.84	0.12	0.24				
Ko-c2	Rhyolitic	Medium-K	76.3	1.8	2.0	76.47	0.46	12.68	2.28	0.13	0.55	2.15	3.43	1.84			10	1*, 2
			-76.8	-1.9	-2.3	0.16	0.07	0.07	0.10	0.07	0.07	0.08	0.10	0.07				
Ta-b	Rhyolitic	Medium-K	74.1	1.9	2.2	75.14	0.39	13.20	2.62	0.07	0.66	2.43	3.32	2.17			10	1*, 2
			-75.8	-2.3	-2.8	0.56	0.06	0.15	0.34	0.06	0.10	0.22	0.26	0.12				
Us-b	Rhyolitic	Low-K	76.3	1.2	1.7	76.90	0.16	13.67	2.00	0.14	0.28	1.76	3.82	1.26			10	1*
			-77.6	-1.5	-2.0	0.36	0.10	0.27	0.18	0.09	0.05	0.09	0.31	0.10				
Ko-d	Rhyolitic	Medium-K	75.1	1.7	2.4	75.07	0.52	13.33	2.45	0.10	0.67	2.74	3.38	1.74			10	1*
			-75.8	-1.9	-2.7	1.17	0.11	0.91	0.18	0.07	0.09	0.62	0.11	0.12				
Ma-b	Rhyolitic	Low-K	74.2	0.7	2.7	74.72	0.68	13.25	2.94	0.13	0.85	2.85	3.81	0.79			10	1*, 2, 3
			-75.3	-0.9	-3.1	0.37	0.08	0.16	0.12	0.10	0.09	0.12	0.22	0.05				
B-Tm	Trachytic-Rhyolitic	High-K	63.1	4.0	0.2	71.97	0.31	12.15	4.25	0.10	0.08	0.60	5.34	4.78	0.03	0.38	66	2, 4*, 5, 6, 7, 8, 9
			-76.1	-6.0	-1.4	4.15	0.15	2.44	0.45	0.04	0.12	0.54	0.49	0.65	0.04	0.17		
SH#12	Rhyolitic	Medium-K	75.6	2.9	1.0	76.75	0.27	12.60	1.18	0.04	0.24	1.13	4.61	3.15	0.04		14	10*, 11
			-77.6	-3.4	-1.5	0.57	0.04	0.47	0.18	0.01	0.03	0.12	0.34	0.13	0.01			
Ta-c	Rhyolitic	Medium-K	73.8	1.9	1.9	76.15	0.39	13.01	2.26	0.05	0.44	2.17	3.35	2.19			10	1*, 2
			-77.1	-2.5	-2.8	1.19	0.05	0.51	0.35	0.08	0.13	0.32	0.18	0.20				
KGP	Rhyolitic	Medium-K	76.5	2.7	1.4	77.14	0.25	12.57	1.20	0.05	0.29	1.61	3.92	2.79	0.05	0.12	19	3*
			-77.6	-2.9	-1.8	0.23	0.04	0.10	0.11	0.04	0.04	0.09	0.09	0.09	0.02	0.02		
SOh	Rhyolitic	Medium-K	74.1	2.4	1.6	75.40	0.19	13.81	1.24	0.07	0.30	1.98	4.02	2.74	0.08	0.18	20	12*, 13
			-76.8	-3.1	-2.5	0.78	0.02	0.55	0.19	0.04	0.09	0.22	0.17	0.03	0.04			
U-2	Phonolitic-Trachytic	High-K	59.4	6.3	1.2	60.54	0.62	19.48	3.16	0.14	0.48	1.99	6.60	6.61	0.17	0.21	19	3*, 14
			-61.8	-7.0	-2.5	0.63	0.07	0.30	0.42	0.10	0.12	0.33	0.60	0.21	0.05	0.04		
To-Cu	Rhyolitic	Low-K	73.4	1.1	2.6	74.15	0.47	13.54	2.33	0.11	0.61	2.81	4.57	1.22	0.08	0.11	25	3*, 15
			-74.4	-1.3	-3.1	0.23	0.03	0.18	0.11	0.05	0.06	0.11	0.15	0.05	0.02	0.02		
Ko-g	Rhyolitic	Medium-K	72.0	1.6	2.7	73.56	0.58	13.26	2.92	0.11	0.71	3.02	4.00	1.72	0.10	0.22	16	1, 2, 10*
			-74.8	-1.8	-3.3	0.66	0.03	0.41	0.18	0.02	0.06	0.17	0.17	0.07	0.01	0.04		
K-Ah	Rhyolitic	Medium-K	70.4	2.3	1.0	73.67	0.56	13.58	2.60	0.09	0.51	2.16	4.01	2.72	0.09		18	13*, 16
			-77.8	-3.5	-3.3	1.47	0.13	0.47	0.48	0.05	0.15	0.45	0.14	0.23	0.04			
Ma-f-j	Dacitic-Rhyolitic	Low-K	70.7	0.6	2.7	73.08	0.69	14.21	3.17	0.14	0.84	3.32	3.81	0.74			20	2*, 10
			-74.4	-0.9	-4.5	1.13	0.09	0.70	0.38	0.11	0.16	0.42	0.18	0.07				
B-Sg-08	Rhyolitic	High-K	74.5	4.4	-0.2	75.01	0.20	10.28	3.89	0.07	0.01	0.20	5.30	4.50	0.01	0.52	25	3*
			-75.3	-4.6		0.18	0.03	0.11	0.10	0.03	0.01	0.02	0.16	0.06	0.01	0.02		
U-3	Phonolitic	High-K	59.6	6.7	1.1	60.52	0.51	19.87	2.81	0.15	0.23	1.48	6.95	7.03	0.05	0.40	24	3*, 14
			-60.8	-7.4	-1.8	0.24	0.08	0.22	0.18	0.03	0.07	0.14	0.40	0.19	0.04	0.08		
Ta-d	Andesitic-Dacitic	Low-K	62.3	0.7	4.5	63.82	0.76	17.31	6.54	0.14	1.83	5.30	3.40	0.90			10	1*
			-65.2	-1.1	-6.4	0.92	0.12	1.29	0.57	0.11	0.23	0.49	0.42	0.11				
U-OkI	Phonolitic-Trachytic	High-K	60.5	6.6	1.4	60.85	0.50	19.55	3.16	0.14	0.30	1.61	6.51	7.07	0.10	0.24	12	14, 17*
			-62.0	-7.5	-2.0	0.42	0.07	0.17	0.19	0.05	0.06	0.17	0.79	0.28	0.03	0.03		

References: 1. Nakamura (2016); 2. Razzhigaeva et al. (2016); 3. McLean et al. (2018); 4. Chen et al. (2016); 5. McLean et al. (2016); 6. Sun et al. (2014); 7. Sun et al. (2015); 8. Hughes et al. (2013); 9. Machida et al. (1990); 10. Chen et al. (2019); 11. Ponomareva et al. (2015); 12. Albert et al. (2018); 13. Smith et al. (2013); 14. Shiihara et al. (2011); 15. Ishimura and Hiramane (2020); 16. Albert et al. (2019); 17. Smith et al. (2011). Asterisks denote where the listed data come from.

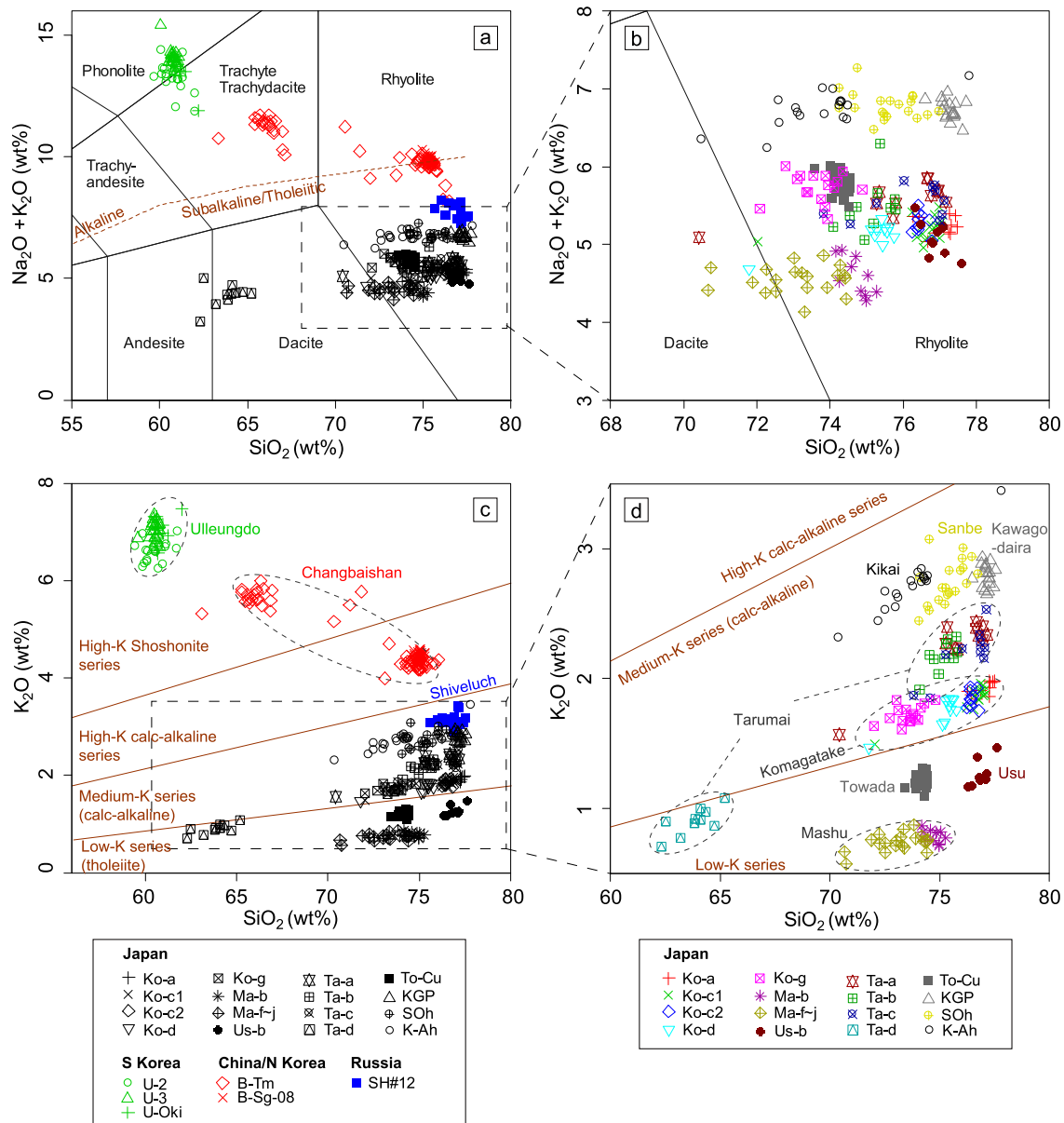


Fig. 2. Glass shard major element compositions of the twenty-two tephra layers within the proposed Holocene tephrostratigraphic framework. (a–b) Total alkaline versus silica (TAS) diagram (classification scheme based on Le Bas et al. (1986)), (c–d) K-classification diagram (classification scheme based on Peccerillo and Taylor (1976)). Note the changes of legend in colour for Japanese tephras in inset (b) and (d), compared to those in (a) and (c). Source volcanoes are indicated in (c–d). For detailed information of each tephra layer see Table 1. Geochemical data sources are listed in Table 2. (For interpretation of the references to colour in this figure legend, the reader is referred to the Web version of this article.)

Shiihara et al., 2011). In contrast, the tephra occurs as visible layers in both Lake Biwa (Nagahashi et al., 2004; Shiihara et al., 2011) and Lake Suigetsu (McLean et al., 2018) on Honshu Island. Glass composition of this tephra is broadly indistinguishable from that of the U-Oki ash in terms of major elements (Table 2; Fig. 2a, c) (McLean et al., 2018), though proximal U-3 glasses show greater geochemical variations compared to proximal U-4 glasses on a FeO_x -CaO bivariate plot (Fig. 3a) (Shiihara et al., 2011). A proximal charcoal sample provides the current best age estimate for the tephra (8440–8360 cal BP (2σ); Im et al., 2012), which has been cross-validated by an independent distal age (8455–8367 cal BP (2σ); McLean et al., 2018).

2.2. Tephra isochrons in mid-holocene (8.2–4.2 ka BP)

The mid-Holocene section of the tephra framework contains six widespread tephra layers. They are the B-Sg-08 tephra from Changbaishan, Ma-f ~ j, Ko-g and To-Cu tephras from northern Japan, K-Ah tephra from southern Japan and U-2 tephra from Ulleungdo (Table 1).

The B-Sg-08 (previously named SG14-1058) is a cryptotephra first identified in Lake Suigetsu, which is sourced from the Changbaishan volcano (Fig. 1) (McLean et al., 2018, 2020). This layer has been linked to a visible layer in a proximal lake (Yuanchi) and suggested to be the distal equivalence of the proximal Qixiangzhan (QXZ) unit of the volcano (Sun et al., 2018). Nevertheless, due to the lack of evidence indicating an explosive phase of the QXZ eruption,

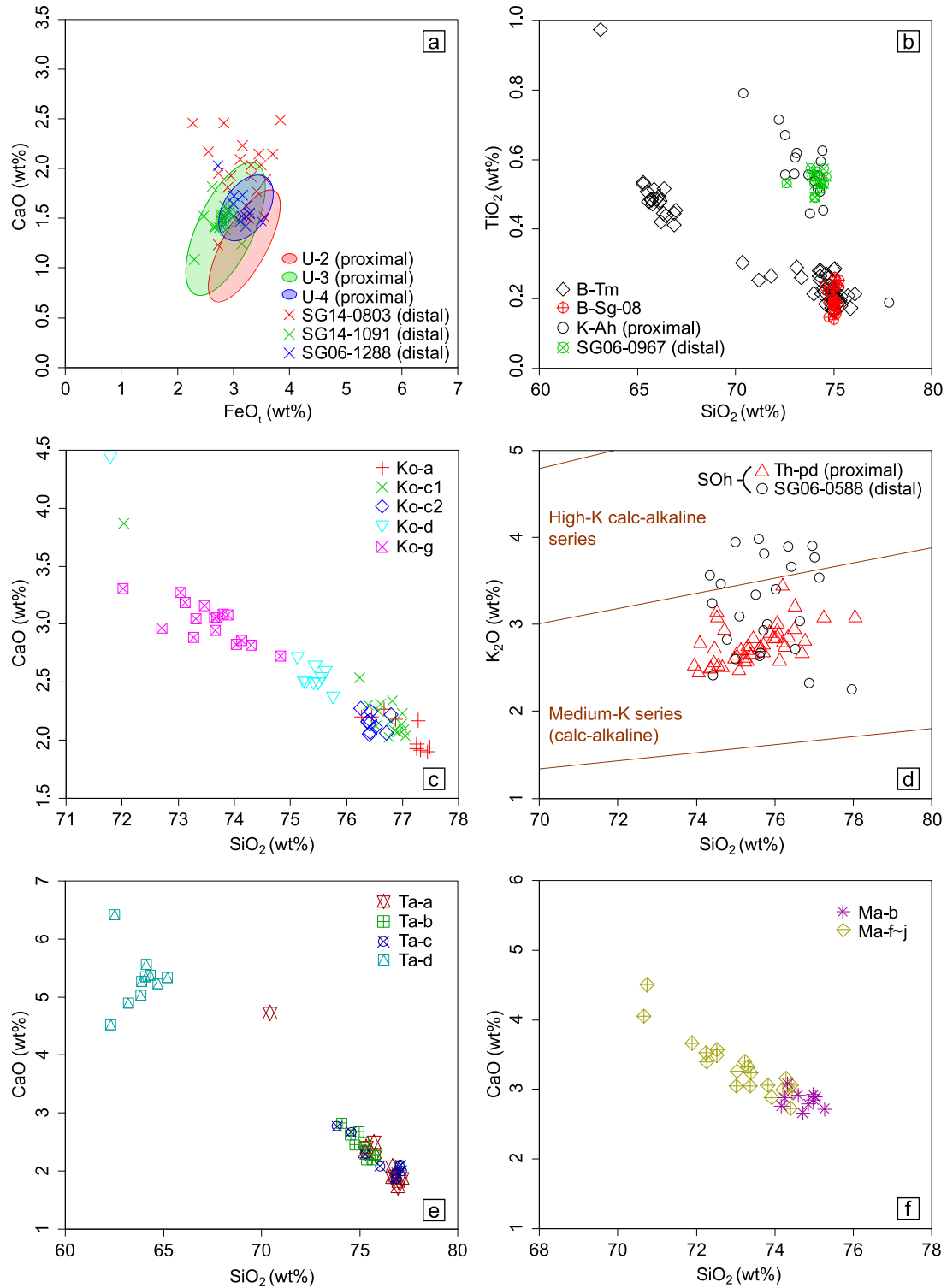


Fig. 3. Glass shard major element compositions of (a) proximal Holocene Ulleungdo tephras (U-2, U-3 and U-4; [Shiuhara et al., 2011](#)) and corresponding distal layers identified in Lake Suigetsu (SG14-0803, SG14-1091 and SG06-1288; [Smith et al., 2011](#); [McLean et al., 2018](#)); (b) distal B-Tm ([Chen et al., 2016](#)) and B-Sg-08 ([McLean et al., 2018, 2020](#)) tephras from Changbaishan volcano, as well as proximal and distal (SG06-0967) K-Ah tephras from Kikai caldera ([Smith et al., 2013](#)); (c) mid-Holocene Ko-g tephra ([Chen et al., 2019](#)) and tephras erupted during historical time periods (Ko-a, Ko-c1, Ko-c2 and Ko-d; [Nakamura, 2016](#)) from Komagatake volcano; (d) proximal (Th-pd) and distal (SG06-0588) SOh tephra from Sanbe volcano ([Albert et al., 2018](#); [Smith et al., 2013](#)); (e) Holocene tephras (Ta-a, Ta-b, Ta-c and Ta-d) from Tarumai volcano ([Nakamura, 2016](#)); and (f) mid-Holocene Ma-f ~ j ([Razzhigaeva et al., 2016](#); [Chen et al., 2019](#)) and late Holocene Ma-b ([Nakamura, 2016](#)) tephras from Mashu volcano.

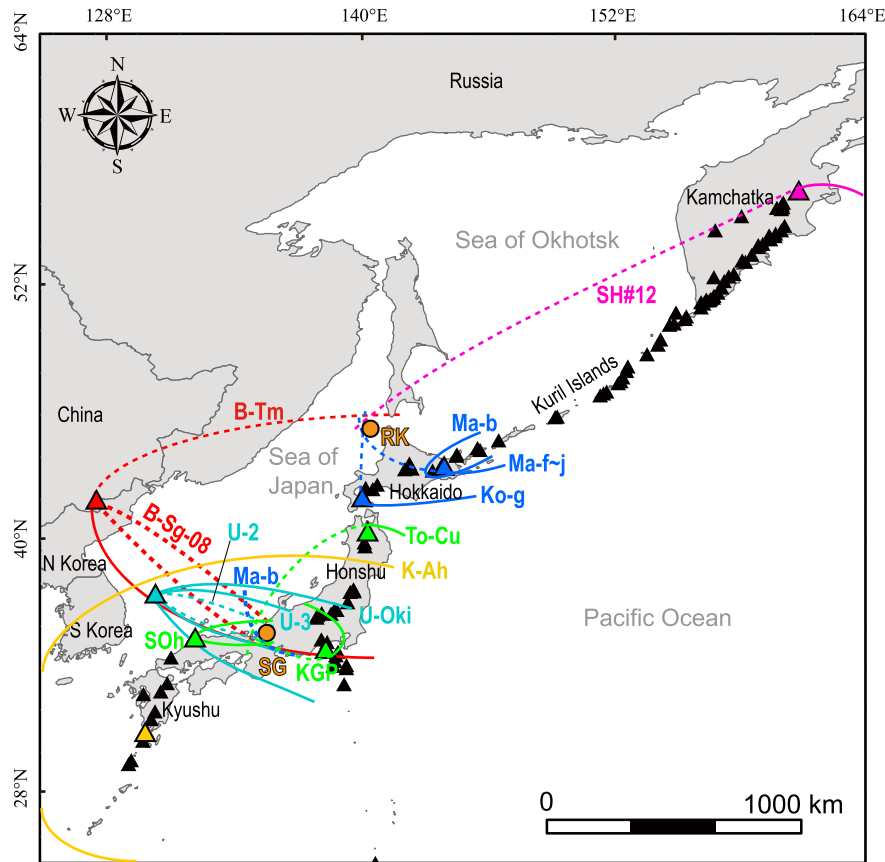


Fig. 4. Map of NE Asia showing up-to-date distribution of the tephra layers within the proposed tephrostratigraphic framework. Note that the distribution of several tephra layers sourced from volcanoes in Hokkaido is not shown. For detailed dispersal of those Hokkaido tephras see Fig. 5. Volcanoes and tephras from different regions are marked using different colours. Solid line indicates that the dispersal limit is based on data from visible tephra studies, whereas dashed line is based on cryptotephra occurrence. The most distant known distribution of each tephra is listed in Table 1. Dispersal data sources include Katsui et al. (1975), Machida and Arai (1983), Machida and Arai (2003), Furukawa and Nanayama (2006), Shiihara et al. (2011), Tani et al. (2013), Razzhigaeva et al. (2016), Nakamura (2016), Chen et al. (2016, 2019), McLean et al. (2016, 2018) and Albert et al. (2018). (For interpretation of the references to colour in this figure legend, the reader is referred to the Web version of this article.)

the suggested QXZ origin for the tephra is yet to be confirmed (McLean et al., 2020; Pan et al., 2020). Glass compositions of the tephra are typical Changbaishan alkaline to subalkaline/tholeiitic rhyolitic (ca. 74.5–75.3 wt% SiO₂; ca. 4.4–4.6 wt% K₂O; Fig. 2) (McLean et al., 2018), which is indistinguishable from the rhyolitic end-member of a younger eruption of the volcano (i.e., B-Tm; Fig. 3b) (Chen et al., 2016). Dated to 8166–8099 cal BP (2σ) (McLean et al., 2018), the tephra presents a potential isochron to link palaeoclimate archives on both sides of the Sea of Japan (Fig. 4), at the transition between the early and mid-Holocene. Nevertheless, a high-resolution cryptotephra study has failed to identify this ash in northern Japan (Chen et al., 2019), suggesting that far more cryptotephra studies are required in the region to test this potential.

The Ma-f ~ j tephra represents the largest Holocene eruption of the Mashu volcano in eastern Hokkaido (Fig. 1). It was dispersed towards the ESE and had a bulk tephra volume of 18.6 km³ (Kishimoto et al., 2009). Previous studies have revealed detailed proximal stratigraphy for this caldera-forming eruption (Katsui et al., 1975; Kishimoto et al., 2009), however, identification of the tephra has long remained in the proximal sites. The furthest known distribution of the visible layer was reported by Razzhigaeva et al. (2016), who traced the ash following its main dispersal axis into the southern Kuril Islands, ca. 200 km away from the volcano. Chen et al. (2019) in contrast, reported the presence of the ash as a cryptotephra in Lake Kushu, Rebun Island ca. 350 km NW of the

Mashu volcano, which is in the opposite direction to the primary plume dispersal (Fig. 4). This indicates that the ash has a much larger distribution area than that was defined by previous visible tephra occurrences, mantling most of the northern Hokkaido and the Kuril arc (Fig. 4). Geochemical analyses reveal that glasses of the tephra are dacitic to rhyolitic (ca. 70.7–74.4 wt% SiO₂; Fig. 2) in composition (Razzhigaeva et al., 2016; Nakamura, 2016; Chen et al., 2019), and possess the lowest K₂O contents (ca. 0.6–0.9 wt% K₂O) among all Japanese tephras within the framework (Fig. 2d). Radiocarbon dating of charcoal sample preserved within the ash layer provides an age of 7670–7480 cal BP (2σ) for the tephra (Yamamoto et al., 2010). Although there are some other dates reported for this tephra (e.g., 7560–7280 cal BP (2σ), Yamamoto et al., 2010; ca. 8.6–8.4 cal ka, Nakamura and Hirakawa, 2004), Bayesian age modelling exercises based on the Lake Kushu sequence suggest that they are less robust (7976–7585 cal BP (2σ) for Ma-f ~ j; Chen, 2019).

The K-Ah tephra from Kikai caldera in southern Kyushu (Fig. 1) is one of the most widespread Holocene tephras in East Asia (Machida and Arai, 1978, 1983; Machida, 1999). Discharging a bulk volume of ca. 170 km³ tephra, the eruption dispersed the ash over 1300 km mantling an area from southern to central Japan, and the adjacent seas (Fig. 4) (Machida and Arai, 1983). Glasses of the tephra are medium-K (ca. 2.3–3.5 wt% K₂O) rhyolitic (ca. 70.4–77.8 wt% SiO₂) (Smith et al., 2013), and they are distinctive among all tephras

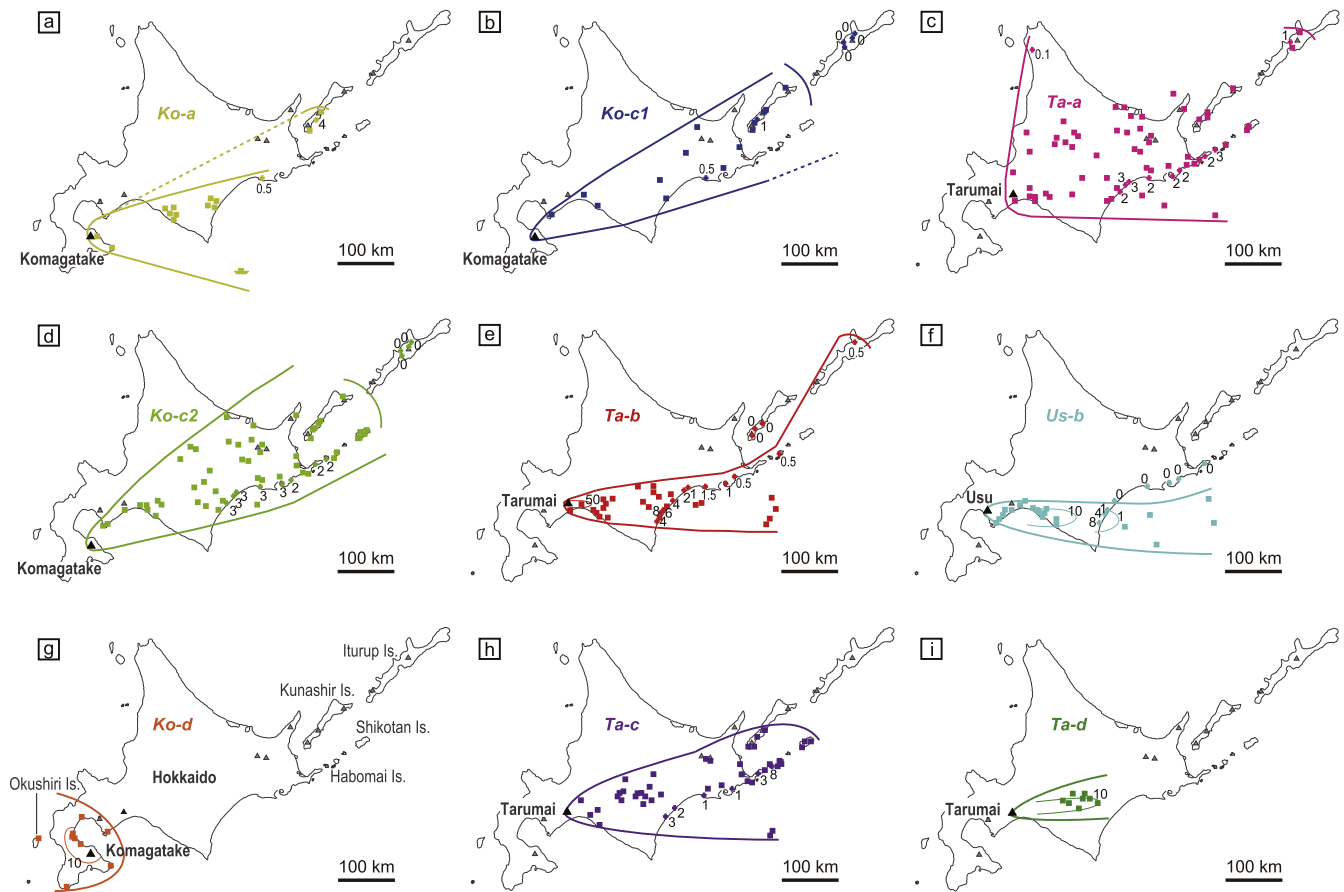


Fig. 5. Map of Hokkaido and southern Kuril Islands showing up-to-date distribution of nine Hokkaido tephras within the proposed tephrostratigraphic framework. Square designates occurrence of the tephra without available thickness data. Cross designates presence of the tephra with a known thickness or absence of the tephra where thickness is zero. Symbol of a cruise ship indicates the area where “pumiceous storm” occurred. The number designates thickness (cm) at the outcrop or for the isopach. Solid line designates confirmed dispersal limit whereas dashed line designates inferred dispersal limit. Dispersal data sources include Machida and Arai (2003), Razzhigaeva et al. (2016), Nakamura (2016), Furukawa and Nanayama (2006) and references therein.

within the framework (Fig. 2). It is worth noting that the proximal K-Ah deposits have greater compositional ranges, which have not been fully observed in the distal layers (e.g., SG06-0967 in Lake Suigetsu; Smith et al., 2013) (Fig. 3b). Detailed investigations are needed to further document these distal-proximal geochemical variations in order to guide future tephra correlations. The eruptive age of the K-Ah has been precisely constrained to 7303–7165 cal BP (2σ) by the Suigetsu SG06 chronology (Staff et al., 2011; Smith et al., 2013). The extensive occurrences of the tephra on land and in the marine environments (e.g., Sea of Japan, Pacific Ocean and East China Sea) allow precise dating of terrestrial and marine sequences, and the test of correction factors for marine reservoir effect.

The Ko-g tephra represents the largest Plinian eruption of the Komagatake volcano in SW Hokkaido (Fig. 1) during the Holocene (Yoshimoto et al., 2008). The tephra was dispersed towards the ENE, covering most of the southern and eastern Hokkaido (Furukawa and Nanayama, 2006). The most distant identification of the visible Ko-g tephra was reported by Razzhigaeva et al. (2016), which extended its known dispersal into the southern Kuril Islands (ca. 450 km). Recently, a cryptotephra study reveals that the Ko-g occurs in Lake Kusu (Chen et al., 2019), confirming the ash actually mantles the entire Hokkaido rather than only its southern and eastern parts (Fig. 4). Glasses of the tephra are medium-K (ca. 1.6–1.8 wt% K_2O) rhyolitic (ca. 72.0–74.8 wt% SiO_2 ; Fig. 2) (Chen et al., 2019; Nakamura, 2016; Razzhigaeva et al., 2016), and they

are distinctive among all Komagatake ashes within the framework owing to their less evolved characteristics (Fig. 3c). Several studies attempted to unravel the age of the tephra, and the results yielded various but overlapping dates (e.g., 6661–6448 cal BP (2σ), Nakamura and Hirakawa, 2004; 7156–6551 cal BP (2σ), Yoshimoto et al., 2008; 6830–6640 cal BP (2σ), calibrated using IntCal13 (Reimer et al., 2013) based on a date from Razzhigaeva et al. (2016)). A recent Bayesian modelling study from Lake Kusu, taking into account all the available chronological, stratigraphic and depositional information, has provided the most robust age estimate for the tephra (6686–6520 cal BP (2σ); Chen, 2019).

The To-Cu tephra represents the largest-volume (ca. 9.2 km³ bulk volume) Plinian eruption of the Towada caldera in northern Honshu (Fig. 1) spanning the Holocene (Hayakawa, 1985). Comprising three sub-units (Chuseri pumice, Kanegasawa pumice and Utarube ash), the eruption dispersed ashes over 150 km to the SE, covering parts of northern Honshu and coastal regions of the Pacific (Hayakawa, 1985; Ishimura and Hiramine, 2020). Among these sub-units, the Chuseri pumice (Cu) has the most distant dispersal. At a locality ca. 500 km WSW of the volcano, the unit has been found with a thickness of 0.2 cm (Ishimura and Hiramine, 2020). A cryptotephra study has increased its known dispersal to ca. 700 km away from the source in central Honshu (Fig. 4) (McLean et al., 2018). Glasses of the tephra are low-K (ca. 1.1–1.3 wt% K_2O) rhyolitic (ca. 73.4–74.4 wt% SiO_2 ; Fig. 2) (McLean et al., 2018;

Ishimura and Hiramine, 2020), and they are compositionally distinctive among all East Asian tephtras within the framework (Fig. 2c). The age of the tephtra varies from study to study. Proximally, Kudo et al. (2003) reported a date of 6282–5926 cal BP (2σ) for soil below To-Cu, whereas Inoue et al. (2011) reported a slightly older age of 6313–6180 cal BP (2σ) for humin within soils below the tephtra. Both the dates are in agreement within error with the age derived from charcoal preserved within the tephtra (6480–5897 cal BP (2σ), calibrated using IntCal13 (Reimer et al., 2013) based on Hayakawa (1983)). Distally, however, the tephtra has been dated to 5986–5899 cal BP (2σ) (McLean et al., 2018), which is slightly younger than those proximal ages.

The U-2 tephtra from Ulleungdo volcano was thought to be generated by a smaller eruption compared to both the U-Oki and U-3 tephtras, as identification of the U-2 has remained in the proximal sites for a long time (e.g., Machida et al., 1984; Shiihara et al., 2011; Kim et al., 2014). Glasses of the tephtra exhibit similar compositions with the older U-Oki and U-3 tephtras (Figs. 2 and 3a) (Shiihara et al., 2011). Recently, McLean et al. (2018) proposed the identification of the distal U-2 horizon in Lake Suigetsu, based on independent chronological evidence, and that the distal layer (SG14-0803) displays typical alkali-rich Ulleungdo chemistry. It is worth noting that, however, the proposed distal U-2 glasses (McLean et al., 2018) show apparently elevated CaO contents (by ca. 1 wt%) compared to the reported proximal U-2 glasses (Shiihara et al., 2011) (Fig. 3a). Further investigations are needed to verify if these obvious CaO offsets truly exist or are due to instrumental/analytical uncertainty. Nevertheless, identification of the U-2 in central Honshu indicates that the ash covers an extensive area in the Sea of Japan, probably as a cryptotephtra layer, given that previous studies did not report this horizon from marine environments (see Shiihara et al., 2011). The age of the tephtra has been dated to 5681–5619 cal BP (2σ) distally (McLean et al., 2018), which is supported by proximal ages derived from charcoal samples preserved within the tephtra layer (e.g., 5734–5600 cal BP (2σ); OKuno et al., 2010).

2.3. Tephtra isochrons in Late Holocene (4.2–0 ka BP)

Thirteen tephtra isochrons are integrated within the tephtra framework spanning the late Holocene period. These include nine major markers from Hokkaido (Ta-c, Ma-b, Ko-d, Us-b, Ta-b, Ko-c2, Ta-a, Ko-c1 and Ko-a), two from Honshu (KGP, SOh), one from China/N Korea (B–Tm), and one from Kamchatka (SH#12) (Table 1).

The oldest tephtra within the late Holocene timeframe is the SOh (Miura and Hayashi, 1991; also named Th-pd, Fukuoka and Matsui, 2002) erupted from Sanbe volcano in SW Honshu (Fig. 1). This eruption has been studied proximally, yet the correlation of volcanic stratigraphy remains controversial (see Fukuoka and Matsui, 2002). Ash from the eruption was thought to be distributed towards the ENE (Fig. 4) (Machida and Arai, 2003). Smith et al. (2013) reported a 0.2 cm thick ash layer (SG06-0588) in Lake Suigetsu, ca. 300 km away from the volcano. This layer has subsequently been correlated to the proximal Th-pd deposit (Albert et al., 2018). In a further south location (Lake Biwa), the ash has been identified as a cryptotephtra horizon (Takemura et al., 2010), which represents the most distant known distribution of the tephtra marker (ca. 320 km). Glass compositions of the tephtra reported proximally are medium-K (ca. 2.4–3.1 wt% K_2O) rhyolitic (ca. 74.1–76.8 wt% SiO_2 ; Fig. 2) (Albert et al., 2018), whereas glasses from distal deposits extend to the high-K series (Fig. 3d) (Smith et al., 2013; Albert et al., 2018). The high-resolution Suigetsu chronology allows a precise age estimate for the tephtra (4068–4004 cal BP (2σ); Albert et al., 2018), which is consistent with published ages derived from charcoals buried in proximal deposits (Fukuoka and Matsui, 2002; and refs therein). Identification of the tephtra would enable the transfer of its

precise age into other sequences.

Erupted from Kawagodaira volcano in SE Honshu (Fig. 1), the KGP/Kg tephtra is the other regional marker originating from central Japan. With a bulk volume of 1.04 km³, the tephtra was mainly dispersed towards the west and covers some large areas of the central and western Honshu (Fig. 4) (Shimada, 2000; Tani et al., 2013). In both Lake Biwa and Lake Suigetsu ca. 300 km to the west of the volcano, the ash occurs as cryptotephtra horizons (Nagahashi et al., 2004; Takemura et al., 2010; McLean et al., 2018). Glasses of the tephtra exhibit medium-K (ca. 2.7–2.9 wt% K_2O) rhyolitic compositions (ca. 76.5–77.6 wt% SiO_2) (McLean et al., 2018), and they are one of the most evolved tephtras within the framework (Fig. 2). The current best age estimate for the ash is provided by radiocarbon wiggle-matching of a Japanese cedar timber found within the associated pyroclastic flow deposit, which dates the eruption to 3160–3137 cal BP (2σ) (Tani et al., 2013). Given its very precise age, the tephtra is crucial for the dating of archaeological sequences of the late and final Jōmon period in the Japanese prehistory.

Postdating the KGP ash, the Ta-c tephtra from Tarumai volcano is one of the major markers in Hokkaido during the late Holocene. Dispersed mainly towards the east, the tephtra has been found covering most of the southern and eastern Hokkaido (Furukawa and Nanayama, 2006; Nakamura, 2016) and has recently been traced into the southern Kuril Islands (Razzhigaeva et al., 2016) (Fig. 5h). Glasses of the ash are medium-K (ca. 1.9–2.5 wt% K_2O) rhyolitic in compositions (ca. 73.8–77.1 wt% SiO_2) (Nakamura, 2016), and they cannot be compositionally discriminated from the younger eruptive phases of the volcano (e.g., Ta-b and Ta-a; Fig. 3e). Consequently, precise correlation of this tephtra requires not only geochemical data but also chronological and/or stratigraphic information. The age of the tephtra is poorly constrained at the moment. Nakamura (2016) provided an age of 2800–2500 cal BP (2σ) based on calibration of previously reported dates. In contrast, Razzhigaeva et al. (2016) proposed a younger age of 2500–2300 cal BP (2σ) for the tephtra. We are not able to determine which age is more reliable due to the lack of detailed information regarding the reported radiocarbon dates. It is worth noting that Mackay et al. (2016) suggested a plausible correlation between a cryptotephtra (FBB12-162) identified in east coast of North America and the Ta-c ash. However, the correlation is not yet confirmed due to the limited amount of analyses on distal shards. More cryptotephtra work in high-resolution records from both the North America and East Asia is needed to verify this potential link.

The SH#12 (SH₁₄₅₀) tephtra is an exotic layer that has, for the first time, been incorporated into the Holocene East Asian tephtra framework. Erupted from the Shiveluch volcano in the Kamchatka Peninsula, Russia (Fig. 1), the tephtra was dispersed towards the SE (Kyle et al., 2011; Ponomareva et al., 2015) and has been identified in a number of localities ca. 50–100 km to the east of the volcano (Ponomareva et al., 2017). Remarkably, Chen et al. (2019) report the occurrence of the ash in Lake Kushu, northern Japan ca. 1900 km from the vent. Importantly, this is the first example of a Holocene Russian tephtra interlinked with Japanese eruptions, which allows connection between East Asia and the further north Kamchatka region to be established (Fig. 4). This has significantly widened the geographical area over which precise correlations of palaeoclimate records can be achieved. In addition, it is reasonable to predict that the tephtra can be traced following its main dispersal axis over 1900 km into the Aleutian Arc, the Bering Sea and probably the SW Alaska, which would serve as a potential correlation tool linking records in NE Asia and North America. Glasses of the tephtra are medium-K (ca. 2.9–3.4 wt% K_2O) rhyolitic (ca. 75.6–77.6 wt% SiO_2) (Chen et al., 2019; Ponomareva et al., 2015), and they can be reliably distinguished from other medium-K rhyolitic Japanese tephtras

within the framework (Fig. 2). The age of the tephra has been dated proximally to 1408–1311 cal BP (2σ) (Ponomareva et al., 2017), which is supported by a slightly more precise age determined distally (1374–1295 cal BP (2σ), Chen et al., 2019).

The B–Tm and the Ma–b tephtras chronologically postdate the SH#12 tephtra and are closely spaced in time (Table 1). The distal B–Tm tephtra was first identified in a number of marine and terrestrial records in Sea of Japan and the islands of Japan (Machida and Arai, 1983) and correlated to the Millennium Eruption of Changbaishan volcano (Machida et al., 1990; Chen et al., 2016). Glass compositions of the tephtra are distinctively high-K and bimodal, ranging from alkaline trachytic to subalkaline/tholeiitic rhyolitic (ca. 63.1–76.1 wt% SiO₂; ca. 4.0–6.0 wt% K₂O; Fig. 2) (Chen et al., 2016; McLean et al., 2016; Sun et al., 2014, 2015). As previously discussed by Chen et al. (2019), these evolved high-K features clearly distinguish them from ashes erupted from other volcanoes in East Asia (Fig. 2). Nevertheless, discrimination between Holocene Changbaishan tephtras (e.g., B–Tm and B–Sg-08) cannot be achieved through either major element glass chemistry (Fig. 3b), or trace element analysis (McLean et al., 2020; Pan et al., 2017, 2020). Consequently, independent chronological data and/or detailed stratigraphic information are essential when correlating ashes from the volcano. Machida (1999) proposes an isopach map for the B–Tm tephtra based on tracing visible ash layer. Recently, the tephtra has been reported from a number of new localities outside the previously known dispersal (Fig. 4), including NE China (Sun et al., 2015), Russian Far East (Razzhigaeva et al., 2019), northern Hokkaido (Chen et al., 2016), central Honshu (McLean et al., 2016), and as far as Greenland (Sun et al., 2014). Moreover, the age of the tephtra has been precisely dated to 946 CE, which is reliably cross-validated by ice-core chronology (Sigl et al., 2015) and ¹⁴C spike-matching dendrochronology (Oppenheimer et al., 2017; Hakozaiki et al., 2018). As such the tephtra provides a valuable isochron for dating and synchronising records between East Asia and Greenland. Given its close association in time with the onset of the Medieval Warm Period (ca. 950–1250 CE; Mann et al., 2009), the tephtra permits the investigation into the timing and phasing of the climatic event across a vast geographic area.

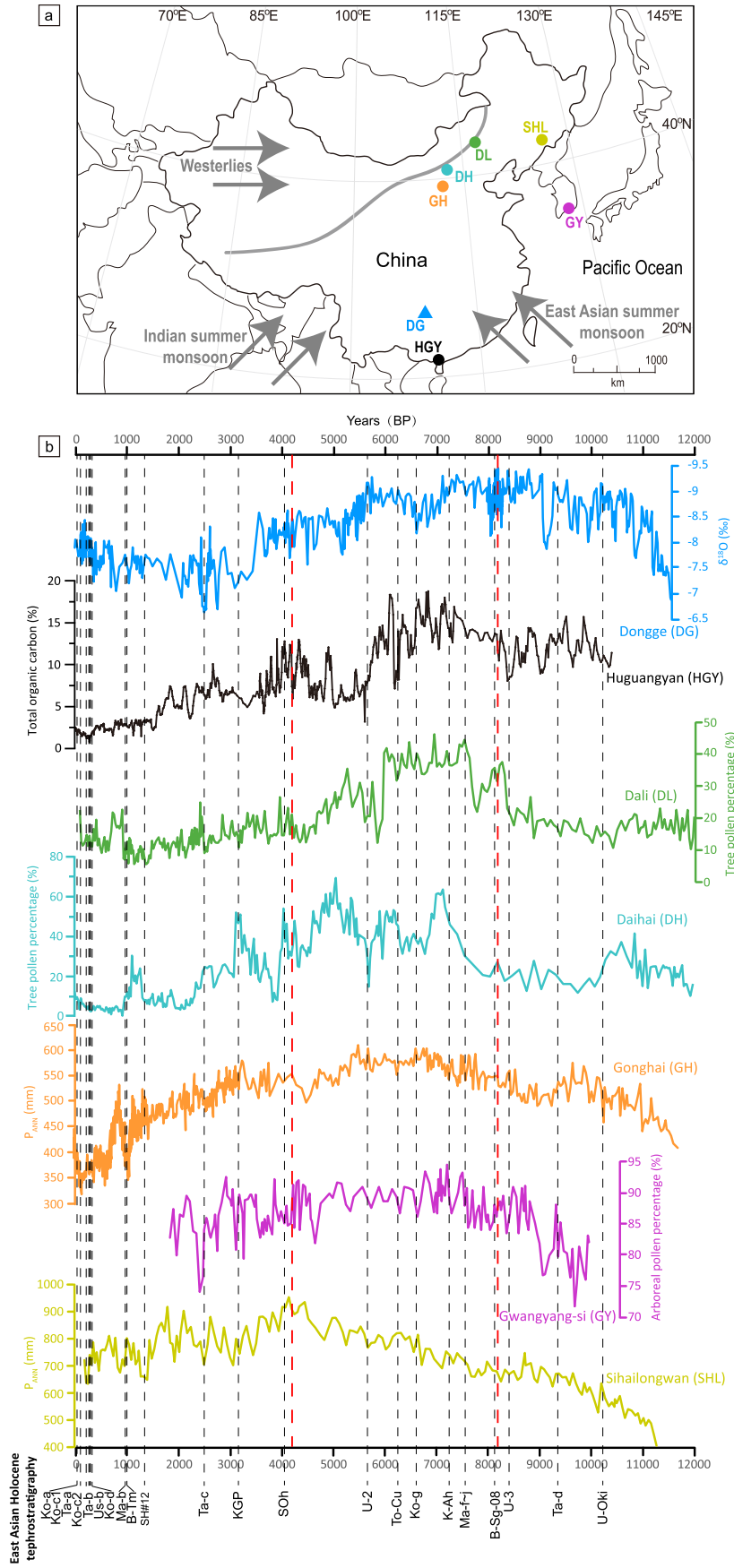
The Ma–b tephtra represents the volumetrically second largest Holocene eruption of the Mashu volcano (Kishimoto et al., 2009). With a bulk volume of 4.6 km³, the tephtra was thought to be dispersed towards the north (Machida and Arai, 2003). Furukawa and Nanayama (2006), however, suggest that the tephtra is more likely to be dispersed easterly, which is supported by Razzhigaeva et al. (2016), who trace the visible ash over 200 km towards the ENE into the southern Kuril Islands (Fig. 4). Subsequently, the ash has been identified as a cryptotephtra horizon in central Honshu (McLean et al., 2018). Over 1100 km SW of Mashu volcano, the new locality is in the opposite direction to the main dispersal axis of the tephtra (Fig. 4), which indicates that the tephtra has a much larger distribution area than that was previously known. Geochemically, glasses of Ma–b tephtra are rhyolitic (ca. 74.2–75.3 wt% SiO₂) and are classified as low-K series (ca. 0.7–0.9 wt% K₂O; Fig. 2) (Nakamura, 2016; Razzhigaeva et al., 2016; McLean et al., 2018). They represent the most evolved components of the Mashu Holocene tephtras (Fig. 3f) (also see Nakamura, 2016). The age of the Ma–b tephtra is best constrained in Lake Suigetsu, where it has been dated to 960–992 CE (2σ) (McLean et al., 2018). Given its close chronostratigraphic relationship with the Medieval Warm Period (ca. 950–1250 CE), the widespread Ma–b tephtra can potentially be used to test the synchronicity of the climate event same as the B–Tm tephtra.

In the uppermost section of the tephrostratigraphic framework, seven major marker tephtras from Hokkaido volcanoes are integrated based on their ages and stratigraphic relationships observed

at outcrops (Nakamura, 2016; Razzhigaeva et al., 2016). They are Ko–d, Us–b, Ta–b, Ko–c2, Ta–a, Ko–c1 and Ko–a dated by historical records to 1640 CE, 1663 CE, 1667 CE, 1694 CE, 1739 CE, 1856 CE and 1929 CE (Table 1), respectively (Oba et al., 1983; Katsui and Komuro, 1984; Nakamura, 2016; and refs therein).

The Ko–d, Ko–c2, Ko–c1 and Ko–a tephtras are from the Komagatake volcano in SW Hokkaido (Fig. 1) and have different dispersal directions (Fig. 5) (Machida and Arai, 2003; Furukawa and Nanayama, 2006; Nakamura, 2016). The Ko–d was known to disperse towards the NW and has been identified over 120 km away from the volcano as a visible layer (Fig. 5g) (Machida and Arai, 2003; Furukawa and Nanayama, 2006). With a bulk volume of 2.9 km³, the tephtra presumably mantles a large area of the north-east Sea of Japan. The Ko–c2 and Ko–c1 tephtras were both dispersed towards the ENE and covered most of the southeastern Hokkaido (Fig. 5b, d) (Machida and Arai, 2003; Furukawa and Nanayama, 2006). Compared to the Ko–c1, the Ko–c2 tephtra has been identified in more outcrops and occurs as a 3-cm-thick layer at a distance of ca. 300 km away from the volcano whereas the Ko–c1 only has a 0.5 cm thickness at the same distance. A recent study has traced the visible Ko–c2 and Ko–c1 layers into Kunashir Island (southern Kuril Islands) over 550 km from the source volcano (Fig. 5b, d) (Razzhigaeva et al., 2016). Nevertheless, both of the tephtras are absent in the further northeast Iturup Island (Fig. 5b, d). The Ko–a tephtra was dispersed towards the ESE and has been identified on land in southern Hokkaido (Fig. 5a). During the Ko–a eruption, pumiceous storm was reported from cruise ship sailing in the Pacific Ocean (Furukawa and Nanayama, 2006). Razzhigaeva et al. (2016) reported visible Ko–a from the Kunashir Island, indicating dispersal of the tephtra is more northerly than previously thought (Fig. 5a). Glasses of these four tephtras erupted during historical time are medium-K rhyolitic in compositions (Fig. 2) (Nakamura, 2016). While the oldest Ko–d tephtra exhibits less evolved characteristics (ca. 75.1–75.8 wt% SiO₂), the three younger ashes (Ko–c2, Ko–c1 and Ko–a) have more evolved (>76 wt% SiO₂) and overlapping major element glass chemistries (Figs. 2d and 3c). Chronological evidence is therefore required for robust correlation of these ashes. In addition, trace element analysis may provide useful tool to aid the discrimination of these Komagatake glasses.

The Us–b tephtra is from the Usu volcano and Ta–b and Ta–a are from the Tarumai volcano. Both of the volcanoes are located in SW Hokkaido (Fig. 1). The Us–b and Ta–b were dispersed towards the east and identified in much of the southern Hokkaido (Fig. 5e and f) (Furukawa and Nanayama, 2006). Both of the tephtras are found over 400 km away from their source volcanoes but the difference is that the Ta–b has been traced into easternmost Hokkaido as a visible layer while the Us–b has not (Fig. 5e and f). As such the Ta–b seems to have a wider distribution compared to the Us–b. A recent study confirms this as the Ta–b has been reported from Iturup Island ca. 600 km away from the Tarumai volcano (Fig. 5e) (Razzhigaeva et al., 2016). This has significantly extended the known distribution of the visible Ta–b tephtra and indicated a more northerly dispersal of the tephtra. The Ta–a was dispersed towards ENE and has the largest volume (4 km³) among the seven tephtras erupted during historical time period (Machida and Arai, 2003). The tephtra was known to cover most of the Hokkaido in a visible form (Fig. 5c) (Furukawa and Nanayama, 2006). Its furthest visible occurrence has been reported from the Iturup Island (ca. 600 km) same as the Ta–b (Fig. 5c, e), but it occurs in more outcrops in the study areas than the Ta–b layer (Razzhigaeva et al., 2016). Compositionally, glasses of the Us–b tephtra are low-K rhyolitic whereas those of the Ta–b and Ta–a are medium-K rhyolitic (Fig. 2; Table 2). The Us–b tephtra exhibits a distinctive composition among all ashes within the framework (Fig. 2d). In contrast, the Ta–b and Ta–a share similar glass compositions though it is unambiguous that the latter



is slightly more felsic (Fig. 3e; Table 2).

3. Potential of tephra isochrons in East Asian palaeoclimate research

Studies on disparate palaeoclimate records have shown that East Asian climate change during the Holocene responds to a complex series of internal forcing factors apart from the orbital forcing (e.g., An et al., 2000). For instance, while the monsoon influenced region of northern China has been more sensitive to changes of ice volume in high northern latitudes (Wen et al., 2017) and intensity of the Westerly winds (Xiao et al., 2004), the monsoonal zone of southern China could have been influenced significantly by the variations of the Atlantic Meridional Overturning Circulation (AMOC) (Wang et al., 2016) and the El Niño–Southern Oscillation (ENSO) (Wang et al., 2007; Wu et al., 2012). In contrast, the coastal East Asian region, including Japan, Korea and eastern China may be largely affected by shifts in western tropical Pacific sea surface temperatures (Park et al., 2019). As a result, it is possible that Holocene climate changes could have had different expressions in different parts of East Asia (Fig. 6).

Chinese speleothem isotopic records have been widely used in global palaeoclimate reconstruction, which is largely attributed to their precise age controls and high temporal resolutions (e.g., Wang et al., 2005, 2008), although interpretations of the $\delta^{18}\text{O}$ signals could still be ambiguous (e.g., Clemens et al., 2010; Maher and Thompson, 2012). $\delta^{18}\text{O}$ record from Dongge Cave, south China (Fig. 6a; Dykoski et al., 2005), has shown that monsoon related precipitation, and thus the summer monsoon intensity, generally tracks changes in solar insolation, but has rapid shifts (i.e., a centennial to multi-decadal scale) that are not evident in insolation variation (Fig. 6b). Enhanced EASM occurred in the early and mid-Holocene for ca. 6 ka (ca. 11.5–5.5 ka BP), whereas the later part of mid-Holocene and the late Holocene experienced significantly reduced monsoon strength. A two-step decline of monsoon intensity was observed gradually during ca. 5.6–5.2 ka BP and rapidly at ca. 3.6 ka BP in ca. 100 years. Abrupt shifts in monsoon intensity occurred throughout the Holocene, four of which at 11.2 ka BP, 10.9 ka BP, 9.2 ka BP, 8.2 ka BP can be linked to cooling events recorded in Greenland ice cores. The observed monsoon variations are assumed to be dominated by solar forcing, with additional internal feedback mechanisms such as AMOC and ENSO involved (Dykoski et al., 2005).

Huguangyan (HGY) is a maar lake located in south China, ca. 500 km to the south of Dongge Cave (Fig. 6a). Total organic carbon (TOC) content of the lake sediment is regarded as a proxy of primary productivity, which increases with enhanced summer monsoon, thus effectively indicating the EASM strength (Shen et al., 2013). The TOC record has shown an enhanced EASM influencing south China before ca. 6 ka BP, which was followed by significant decline of the monsoon strength afterwards (Fig. 6b; Wu et al., 2012). The pattern of monsoon variability recorded in the lake is very similar to that of the Dongge cave, both of which reveal dramatic declines of monsoon strength between ca. 6–5 ka BP and ca. 4–3 ka BP, as well as centennial scale climatic shifts in the early Holocene (e.g., 9.2 ka and 8.2 ka events). Nevertheless, questions such as to what extent these monsoon changes can be correlated,

and the precise chronological constraint on leads and lags of rapid climate shifts in different records cannot be accessed in detail at the moment, which is largely due to the centennial scale errors in lacustrine ^{14}C chronology (see Wu et al., 2012). It is apparent that many of the ash layers in the proposed tephra framework chronologically bracket or are closely associated with those climatic shift events. For instance, the mid-Holocene To–Cu and U–2 tephras bracket the sharp decrease of TOC content began in ca. 6.1 ka in the HGY record, whereas the U–2 tephra is positioned close to the onset of the correlated shift in $\delta^{18}\text{O}$ signal in Dongge Cave. In addition, the B–Sg–08 and U–3 tephras seem to be associated in time with the 8.2 ka signal in Dongge and HGY records, respectively (Fig. 6b). Although these tephra layers cannot be recovered from cave deposits, their identification in the HGY record has great potential to refine the existing ^{14}C chronology and more importantly, will significantly enhance the ability of the HGY archive to be synchronised to other high resolution lacustrine records, which is fundamental for characterising regional variations of abrupt climate changes.

Dali Lake and Daihai Lake are both located in northern China, near the modern EASM limit (Fig. 6a). In these records, the proportion of tree and shrub pollen is thought to be a reliable proxy for precipitation, thus representing summer monsoon intensity (Wen et al., 2017; Xiao et al., 2004). Compared to records from south China (e.g., Dongge and HGY), which suggest the maximum summer monsoon intensity occurred in the early to mid-Holocene before ca. 6 ka BP, the two records from northern China show an unambiguous HO during the mid-Holocene (Fig. 6b). In the Dali Lake record, the EASM intensified significantly at ca. 8.3 ka BP and maintained a high level until ca. 6 ka BP and then decreased rapidly, which turns out to be very similar with the pattern recorded in HGY during the mid-Holocene. The U–3 tephra appears to mark the onset of this monsoon intensification period in both the Dali and HGY records, which permits detailed investigation into the relative timing and phasing of this climatic event. Similarly, the To–Cu and U–2 tephras can be used to constrain the rapid decline of monsoon intensity at ca. 6 ka BP in both of the records.

In the Daihai Lake record, the maximum monsoon intensity occurs between ca. 7.5 ka BP and ca. 4.0 ka BP, which is perfectly bracketed chronologically by the Ma–f ~ j and SOh tephras (Fig. 6b). During this period, decadal to centennial scale climate shifts occurred, and mid-Holocene tephra layers such as U–2, To–Cu and Ko–g could be used to constrain the precise timing of such events once they were identified in the record. It is also very interesting that the pattern of monsoon variation during the mid-Holocene recorded in the Daihai and Dali lakes are quite different, despite the facts that the two lakes are both located in northern China, and that the reconstructions are based on the same type of proxy (i.e., tree pollen percentage). For example, a transition at ca. 6 ka BP from a warm and humid climate to a cooler and drier condition, as recorded in the Dali Lake, is not evident in the Daihai record. This indicates significant regional variations exist within the monsoonal region of northern China. During the late Holocene, the Daihai record also exhibits centennial scale climate anomalies indicated by elevated monsoon strength which are not seen in the Dali record (Fig. 6b). Importantly, late Holocene tephra layers SOh, KGP, Ta–c, SH#12 and B–Tm are all chronologically associated with these

Fig. 6. A compilation of high resolution palaeoclimate proxy records from East Asia plotted against the proposed tephrostratigraphic framework, with a map (after Dykoski et al., 2005) showing locations of the related archives as well as monsoon and westerly wind pathways. The triangle and circles in (a) indicate locations of cave and lakes, respectively, and the colours match with the corresponding proxy records in (b). The grey solid line in (a) designates the modern East Asian summer monsoon limit. The red dashed lines in (b) indicate the boundaries between the early, middle and late Holocene following Walker et al. (2019). The proxy records are plotted on their independent timescales, with data from Dykoski et al. (2005), Wu et al. (2012), Wen et al. (2017), Xiao et al. (2004), Chen et al. (2015), Park et al. (2019) and Stebich et al. (2015). The chronostratigraphic position of the tephra layer is based on the median value of its age range. For age ranges and data sources see Table 1. (For interpretation of the references to colour in this figure legend, the reader is referred to the Web version of this article.)

climate anomalies and thus can be used to verify and constrain the timing of such rapid climate changes.

Gonghai Lake is also located in northern China, to the south of the Dali and Daihai lakes (Fig. 6a). Pollen data from Gonghai are transferred quantitatively into annual precipitation, for providing a direct record of monsoon rainfall (Chen et al., 2015). Variations of summer monsoon intensity recorded in this site are generally more gradual than other records (Fig. 6b). A millennial scale precipitation decline event at ca. 9.5–8.5 ka BP has been recognised (Chen et al., 2015), which broadly corresponds to several rapid monsoon decline events spanning 9.2–8.4 ka BP reported from the HGY sequence. The Ta-d and U-3 tephtras in the proposed framework appropriately bracket this climate change period, and thus provide important isochrons for interregional proxy data comparison. The Gonghai record also reveals that the Holocene maximum EASM precipitation occurred in mid-Holocene at ca. 7.8–5.3 ka BP, and a persistent decline of monsoon strength happened from ca. 3.3 ka BP. Interestingly, the KGP tephra chronologically coincides with the onset of this progressive monsoon deterioration. In addition, both the Gonghai and Dali sequences in northern China record a major climate anomaly during the last 1 ka, indicated by centennial scale and large-amplitude precipitation increase, which can be correlated to the globally recognised Medieval Warm Period (MWP) spanning ca. 1.0–0.7 ka BP (Mann et al., 2009). The hemispheric scale tephra marker B–Tm and the regional scale marker Ma-b both fall closely to the onset of the MWP, which allow the test of the synchronicity of this widespread climatic phenomenon across different regions.

A high resolution pollen record from Gwangyang-si (GY), coastal area of South Korea (Fig. 6a; Park et al., 2019), corroborates the mid-Holocene summer monsoon maximum revealed by other records from northern China. The GY pollen record shows a maximal EASM period at ca. 7.6–4.8 ka BP (Fig. 6b), which broadly overlaps with that of the Gonghai record (ca. 7.8–5.3 ka BP). The Ma-f ~ j tephra falls right at the onset of this HO period in the GY record based on current chronologies. Its identification in the record will allow better constraint on the timing of this climate event, as well as verification of the current GY ^{14}C chronology. In addition to the HO, the GY record also reveals several centennial scale drying events, indicated by significantly reduced arboreal pollen percentage, centred at ca. 9.7 ka BP, 9.2 ka BP, 4.7 ka BP, 3.2 ka BP and 2.4 ka BP. The Ta-d, KGP and Ta-c tephtras are positioned close to the 9.2 ka BP, 3.2 ka BP and 2.4 ka BP events, respectively. As such, the markers have the potential to unravel the precise timing of those abrupt climate shifts.

Sihailongwan (SHL) is a maar lake located in NE China (Fig. 6a) with annually laminated sediments (Stebich et al., 2015). Annual precipitation reconstructed using pollen data from the site indicates a summer monsoon evolution pattern that is significantly different from those of the monsoonal regions of southern and northern China (Fig. 6b). Monsoon related precipitation shows a long-term increasing trend since the beginning of the Holocene and reaches its maximum value at ca. 4.0 ka BP. The SOh tephra appears to chronologically coincide with this important turning point, since which the monsoon precipitation starts decreasing (Fig. 6b). It is noteworthy that variability of the EASM increases dramatically during the late Holocene in this record, which is marked by numerous rapid shifts in annual precipitation with larger amplitude compared to those in the early to mid-Holocene (Fig. 6b). Late Holocene tephra layers such as Ta-c, SH#12, B–Tm, Ma-b, Ko-c2 and Ta-a are all chronologically associated with the rapid change events, and thus are useful for proxy data comparison.

In summary, records from East Asia exhibit a wide range of patterns regarding the evolution of EASM spanning the Holocene. This has given rise to a fundamental challenge in future research,

which is the robust integration of various site-specific palaeoclimate records. The widely used ^{14}C method provides chronological frameworks for most of the sedimentary sequences, but its inherent dating errors, usually centennial in scale (e.g., Telford et al., 2004; Blockley et al., 2007), prevent detailed investigations into regional variations of abrupt climate changes. A comprehensive regional tephra framework containing a number of widely dispersed tephra layers, has great potential for providing an independent tool for precise dating and synchronisation of disparate records. To this end, it is essential to identify tephra markers within the framework in as many key natural archives as possible. This could lead to a better understanding of how regional environments respond to rapid climate changes, as well as the role of various external and internal forcings in influencing regional climates.

4. Concluding remarks

In light of the recent identification of East Asian cryptotephra layers in Greenland (Sun et al., 2014; Bourne et al., 2016) and probably North America (Mackay et al., 2016), and the identification of a Russian cryptotephra in northern Japan (Chen et al., 2019), East Asia is an ideal region for the search of widespread tephra layers that are important for the synchronisation of palaeoclimate records. The Holocene tephra framework presented here is, thus, a basis for future tephra studies and represents an essential step forward towards a master Holocene tephrostratigraphy for East Asia. A total of twenty-two ash layers have been selected and integrated into the framework, with their associated geochemical, chronological and dispersal data thoroughly discussed. These have been evaluated alongside high resolution palaeoclimate records from the region, demonstrating the significant potential of tephra isochrons in assessing the relative timing and phasing of rapid monsoon changes, which are crucial for understanding the monsoon dynamics. However, the recovery of these tephra layers in well-resolved palaeoclimate archives from the region is inadequate, which is due to the very limited applications of the cryptotephra separation techniques. Therefore, an urgent focus for future research is the necessity to systematically search for cryptic hidden tephra layers in sedimentary sequences from the region. Finally, while we have discussed the need to add in additional chronological information to distinguish tephtras, where major elements are not sufficient to discriminate between ashes from the same volcano, it is also important in the future to test the potential for trace element analyses in this region to act as an additional discrimination tool.

Author contributions

Xuan-Yu Chen: Conceptualization; Data curation; Investigation; Visualization; Writing - original draft; Writing - review & editing. **Simon P.E. Blockley:** Conceptualization; Validation; Writing - review & editing; Supervision. **Yi-Gang Xu:** Writing - review & editing; Supervision; Funding acquisition. **Martin A. Menzies:** Writing - review & editing; Supervision; Project administration.

Declaration of competing interest

The authors declare no competing interests.

Acknowledgements

This study was supported by Chinese Academy of Sciences Strategic Priority Research Program (B) (XDB18000000) and the External Cooperation Program of Bureau of International Cooperation, CAS (Grant No. 132744KYSB20130005). XYC's stay at

RHUL was supported by the collaboration scheme between GIGCAS and RHUL. We would like to thank Dr Yugo Nakamura, Dr Akiko Matsumoto and Dr Miki Shiihara for providing full dataset of glass chemistry from their published papers; Dr Jungjae Park for providing full dataset of pollen percentage from his published paper. We are grateful to Dr Junting Qiu for his help with accessing Japanese literature, Dr Cong Chen and Dr Danielle McLean for beneficial discussions, and Dr Yajun Li for sharing collected data from literature. We would like to extend our thanks to the two anonymous reviewers for their feedback on an earlier version of the manuscript, and to Dr Giovanni Zanchetta for handling the manuscript. This is contribution No. IS-2882 from GIGCAS.

Appendix A. Supplementary data

Supplementary data to this article can be found online at <https://doi.org/10.1016/j.quascirev.2020.106467>.

References

- Abbott, P.M., Davies, S.M., 2012. Volcanism and the Greenland ice-cores: the tephra record. *Earth Sci. Rev.* 115 (3), 173–191.
- Abbott, P.M., Griggs, A.J., Bourne, A.J., Chapman, M.R., Davies, S.M., 2018. Tracing marine cryptotephra in the North Atlantic during the last glacial period: improving the North Atlantic marine tephrostratigraphic framework. *Quat. Sci. Rev.* 189, 169–186.
- Albert, P.G., Smith, V.C., Suzuki, T., Tomlinson, E.L., Nakagawa, T., McLean, D., Yamada, M., Staff, R.A., Scholout, G., Takemura, K., 2018. Constraints on the frequency and dispersal of explosive eruptions at Sambe and Daisen volcanoes (South-West Japan Arc) from the distal Lake Suigetsu record (SG06 core). *Earth Sci. Rev.* 185, 1004–1028.
- Albert, P.G., Smith, V.C., Suzuki, T., McLean, D., Tomlinson, E.L., Miyabuchi, Y., Kitaba, I., Mark, D.F., Moriwaki, H., Nakagawa, T., 2019. Geochemical characterisation of the Late Quaternary widespread Japanese tephrostratigraphic markers and correlations to the Lake Suigetsu sedimentary archive (SG06 core). *Quat. Geochronol.*
- An, Z., 2000. The history and variability of the East Asian paleomonsoon climate. *Quat. Sci. Rev.* 19 (1), 171–187.
- An, Z., Porter, S.C., Kutzbach, J.E., Xihao, W., Suming, W., Xiaodong, L., Xiaoqiang, L., Weijian, Z., 2000. Asynchronous holocene optimum of the east asian monsoon. *Quat. Sci. Rev.* 19 (8), 743–762.
- Aoki, K., Arai, F., 2000. Late Quaternary tephrostratigraphy of marine core KH94-3, LM-8 off Sanriku, Japan. *The Quaternary Research (Daiyonki-kenkyu)* 39 (2), 107–120 (in Japanese with English abstract).
- Aoki, K., Irino, T., Oba, T., 2008. Late Pleistocene tephrostratigraphy of the sediment core MD01-2421 collected off the Kashima coast, Japan. *The Quaternary Research (Daiyonki-kenkyu)* 47, 391–407 (in Japanese with English abstract).
- Arai, F., Machida, H., Okumura, K., Miyauchi, T., Soda, T., Yamagata, K., 1986. Catalog for late quaternary marker-tephras in Japan ii : tephra occurring in northeast honshu and hokkaido. *Geogr. Rep. Tokyo Metropol. Univ.* 21, 223–250.
- Berben, S.M.P., Dokken, T.M., Abbott, P.M., Cook, E., Sadatzki, H., Simon, M.H., Jansen, E., 2020. Independent tephrochronological evidence for rapid and synchronous oceanic and atmospheric temperature rises over the Greenland stadial-interstadial transitions between ca. 32 and 40 ka b2k. *Quat. Sci. Rev.* 236, 106277.
- Blockley, S.P.E., Pyne-O'Donnell, S.D.F., Lowe, J.J., Matthews, I.P., Stone, A., Pollard, A.M., Turney, C.S.M., Molyneux, E.G., 2005. A new and less destructive laboratory procedure for the physical separation of distal glass tephra shards from sediments. *Quat. Sci. Rev.* 24 (16–17), 1952–1960.
- Blockley, S.P.E., Blaauw, M., Bronk Ramsey, C., van der Plicht, J., 2007. Building and testing age models for radiocarbon dates in Lateglacial and Early Holocene sediments. *Quat. Sci. Rev.* 26 (15), 1915–1926.
- Blockley, S.P.E., Bourne, A.J., Brauer, A., Davies, S.M., Hardiman, M., Harding, P.R., Lane, C.S., MacLeod, A., Matthews, I.P., Pyne-O'Donnell, S.D.F., Rasmussen, S.O., Wulf, S., Zanchetta, G., 2014. Tephrochronology and the extended intimate (integration of ice-core, marine and terrestrial records) event stratigraphy 8–128 ka b2k. *Quat. Sci. Rev.* 106, 88–100.
- Blockley, S.P.E., Edwards, K.J., Schofield, J.E., Pyne-O'Donnell, S.D.F., Jensen, B.J.L., Matthews, I.P., Cook, G.T., Wallace, K.L., Froese, D., 2015. First evidence of cryptotephra in palaeoenvironmental records associated with Norse occupation sites in Greenland. *Quat. Geochronol.* 27, 145–157, 0.
- Bourne, A., Lowe, J., Trincardi, F., Asioli, A., Blockley, S., Wulf, S., Matthews, I., Piva, A., Vigliotti, L., 2010. Distal tephra record for the last ca 105,000 years from core PRAD 1-2 in the central Adriatic Sea: implications for marine tephrostratigraphy. *Quat. Sci. Rev.* 29 (23), 3079–3094.
- Bourne, A.J., Cook, E., Abbott, P.M., Seierstad, I.K., Steffensen, J.P., Svensson, A., Fischer, H., Schüpbach, S., Davies, S.M., 2015. A tephra lattice for Greenland and a reconstruction of volcanic events spanning 25–45 ka b2k. *Quat. Sci. Rev.* 118, 122–141.
- Bourne, A.J., Abbott, P.M., Albert, P.G., Cook, E., Pearce, N.J.G., Ponomareva, V., Svensson, A., Davies, S.M., 2016. Underestimated risks of recurrent long-range ash dispersal from northern Pacific Arc volcanoes. *Sci. Rep.* 6, 29837.
- Chen, X.-Y., 2019. The Holocene Cryptotephra Record of Lake Kushu, Northern Japan: towards an Integrated Tephrostratigraphic Framework for East Asia. Royal Holloway, University of London, p. 216.
- Chen, F., Xu, Q., Chen, J., Birks, H.J.B., Liu, J., Zhang, S., Jin, L., An, C., Telford, R.J., Cao, X., 2015. East Asian summer monsoon precipitation variability since the last deglaciation. *Sci. Rep.* 5, 11186.
- Chen, X.-Y., Blockley, S.P.E., Tarasov, P.E., Xu, Y.-G., McLean, D., Tomlinson, E.L., Albert, P.G., Liu, J.-Q., Müller, S., Wagner, M., Menzies, M.A., 2016. Clarifying the distal to proximal tephrochronology of the Millennium (B-Tm) eruption, Changbaishan Volcano, northeast China. *Quat. Geochronol.* 33, 61–75.
- Chen, X.-Y., McLean, D., Blockley, S.P.E., Tarasov, P.E., Xu, Y.-G., Menzies, M.A., 2019. Developing a holocene tephrostratigraphy for northern Japan using the sedimentary record from lake Kushu, Rebus island. *Quat. Sci. Rev.* 215, 272–292.
- Clemens, S.C., Prell, W.L., Sun, Y., 2010. Orbital-scale timing and mechanisms driving Late Pleistocene Indo-Asian summer monsoons: reinterpreting cave speleothem $\delta^{18}O$. *Paleoceanography* 25 (4).
- Cook, E., Portnyagin, M., Ponomareva, V., Bazanova, L., Svensson, A., Garbe-Schönberg, D., 2018. First identification of cryptotephra from the Kamchatka Peninsula in a Greenland ice core: implications of a widespread marker deposit that links Greenland to the Pacific northwest. *Quat. Sci. Rev.* 181, 200–206.
- Davies, S.M., Abbott, P.M., Pearce, N.J.G., Wastegård, S., Blockley, S.P.E., 2012. Integrating the INTIMATE records using tephrochronology: rising to the challenge. *Quat. Sci. Rev.* 36, 11–27.
- Davies, S.M., Abbott, P.M., Meara, R.H., Pearce, N.J.G., Austin, W.E.N., Chapman, M.R., Svensson, A., Bigler, M., Rasmussen, T.L., Rasmussen, S.O., Farmer, E.J., 2014. A North Atlantic tephrostratigraphical framework for 130–60 ka b2k: new tephra discoveries, marine-based correlations, and future challenges. *Quat. Sci. Rev.* 106, 101–121.
- Davies, L.J., Jensen, B.J.L., Froese, D.G., Wallace, K.L., 2016. Late Pleistocene and Holocene tephrostratigraphy of interior Alaska and Yukon: key beds and chronologies over the past 30,000 years. *Quat. Sci. Rev.* 146, 28–53.
- Domitsu, H., Shiihara, M., Torii, M., Tsukawaki, S., Oda, M., 2002. Tephrostratigraphy of the piston cored sediment KT96-17 P-2 in the southern Japan Sea-the eruption age of Daisen-Kusadanihara Pumice (KsP). *J. Geol. Soc. Jpn.* 108 (9), 545–556.
- Dykoski, C.A., Edwards, R.L., Cheng, H., Yuan, D., Cai, Y., Zhang, M., Lin, Y., Qing, J., An, Z., Revenaugh, J., 2005. A high-resolution, absolute-dated Holocene and deglacial Asian monsoon record from Dongge Cave, China. *Earth Planet. Sci. Lett.* 233 (1), 71–86.
- Fukuoka, T., Matsui, S., 2002. Stratigraphy of pyroclastic deposits post-dating the AT tephra, Sambe volcano. *Earth Science (Chikyū Kagaku)* 56, 105–122 (in Japanese with English abstract).
- Furukawa, R., Nanayama, F., 2006. Holocene pyroclastic fall deposits along the Pacific coastal region of eastern Hokkaido. *Bull. Volcanol. Soc. Jpn.* 51 (6), 351–371 (in Japanese with English abstract).
- Furuta, T., Fujioka, K., Arai, F., 1986. Widespread submarine tephra around Japan — petrographic and chemical properties. *Mar. Geol.* 72 (1), 125–142.
- Hakozaki, M., Miyake, F., Nakamura, T., Kimura, K., Masuda, K., Okuno, M., 2018. Verification of the annual dating of the 10th century Baitoushan volcano eruption based on an ad 774–775 radiocarbon spike. *Radiocarbon* 60 (1), 261–268.
- Hayakawa, Y., 1983. Chuseri tephra formation from Towada volcano, Japan. *Bull. Volcanol. Soc. Jpn.* 28, 263–273 (in Japanese with English abstract).
- Hayakawa, Y., 1985. Pyroclastic geology of Towada volcano. *Bull. Earthq. Res. Inst. Univ. Tokyo* 60, 507–592.
- Hughes, P.D.M., Mallon, G., Brown, A., Essex, H.J., Stanford, J.D., Hotes, S., 2013. The impact of high tephra loading on late-Holocene carbon accumulation and vegetation succession in peatland communities. *Quat. Sci. Rev.* 67, 160–175, 0.
- Ikehara, K., 2015. Marine tephra in the Japan Sea sediments as a tool for paleoceanography and paleoclimatology. *Progress in Earth and Planetary Science* 2 (1), 36.
- Ikehara, K., Usami, K., Kanamatsu, T., Danhara, T., Yamashita, T., 2017. Three important Holocene tephra off the Pacific coast of the Tohoku region, Northeast Japan: implications for correlating onshore and offshore event deposits. *Quat. Int.* 456, 138–153.
- Im, J.H., Shim, S.H., Choo, C.O., Jang, Y.D., Lee, J.S., 2012. Volcanological and paleo-environmental implications of charcoals of the nari formation in nari caldera, ulleung island, Korea. *Geosci. J.* 16 (2), 105–114.
- Inoue, Y., Hiradate, S., Sase, T., Hosono, M., Morita, S., Matsuzaki, H., 2011. Using ^{14}C dating of stable humin fractions to assess upbuilding pedogenesis of a buried Holocene humic soil horizon, Towada volcano, Japan. *Geoderma* 167–168, 85–90.
- Ishimura, D., Hiramine, R., 2020. Proximal–distal fall deposit correlation of VEI-5 tephra (Towada-Chuseri) from Towada volcano, northeast Japan. *J. Quat. Sci.* 35 (1–2), 334–348.
- Jensen, B.J., Pyne-O'Donnell, S., Plunkett, G., Froese, D.G., Hughes, P.D., Sigl, M., McConnell, J.R., Amesbury, M.J., Blackwell, P.G., van den Bogaard, C., Buck, C.E., Charman, D.J., Clague, J.J., Hall, V., Koch, J., Mackay, H., Mallon, G., McCol, L., Pilcher, J.R., 2014. Transatlantic distribution of the Alaskan white river ash. *Geology* 42 (10), 875–878.
- Katsui, Y., Komuro, H., 1984. formation of fractures in Komagatake volcano, hokkaido. *J. Fac. Sci. Hokkaido Univ. - Ser. 4 Geol. Mineral.* 21 (2), 183–195.

- Katsui, Y., Ando, S., Inaba, K., 1975. Formation and magmatic evolution of Mashu volcano, east Hokkaido, Japan. *J. Fac. Sci. Hokkaido Univ. - Ser. 4 Geol. Mineral.* 16 (4), 533–552.
- Kim, G., Cronin, S., Yoon, W., Sohn, Y., 2014. Post 19 ka BP eruptive history of Ulleung Island, Korea, inferred from an intra-caldera pyroclastic sequence. *Bull. Volcanol.* 76 (4), 802.
- Kishimoto, H., Hasegawa, T., Nakagawa, M., Wada, K., 2009. Tephrostratigraphy and eruption style of Mashu volcano, during the last 14,000 years, eastern Hokkaido, Japan. *Bull. Volcanol. Soc. Jpn.* 54, 15–36 (in Japanese with English abstract).
- Kudo, T., Okuno, M., Nakamura, T., 2003. Eruptive history of Kita-Hakkoda volcanic group during the last 6000 years, Northeast Japan. *J. Geol. Soc. Jpn.* 109 (3), 151–165 (in Japanese with English abstract).
- Kyle, P.R., Ponomareva, V.V., Rourke Schluep, R., 2011. Geochemical characterization of marker tephra layers from major Holocene eruptions, Kamchatka Peninsula, Russia. *Int. Geol. Rev.* 53 (9), 1059–1097.
- Lane, C.S., Blockley, S.P.E., Mangerud, J., Smith, V.C., Lohne, Ø.S., Tomlinson, E.L., Matthews, I.P., Lotter, A.F., 2012. Was the 12.1 ka Icelandic Vedde Ash one of a kind? *Quat. Sci. Rev.* 33, 87–99, 0.
- Lane, C.S., Brauer, A., Blockley, S.P.E., Dulski, P., 2013a. Volcanic ash reveals time-transgressive abrupt climate change during the Younger Dryas. *Geology* 41 (12), 1251–1254.
- Lane, C.S., Chorn, B.T., Johnson, T.C., 2013b. Ash from the Toba supereruption in Lake Malawi shows no volcanic winter in East Africa at 75 ka. *Proc. Natl. Acad. Sci. Unit. States Am.* 110 (20), 8025.
- Lane, C.S., Brauer, A., Martín-Puertas, C., Blockley, S.P.E., Smith, V.C., Tomlinson, E.L., 2015. The Late Quaternary tephrostratigraphy of annually laminated sediments from Meerfelder Maar, Germany. *Quat. Sci. Rev.* 122, 192–206.
- Le Bas, M.J., Le Maitre, R.W., Streckeisen, A., Zanettin, B., 1986. A chemical classification of volcanic rocks based on the total alkali-silica diagram. *J. Petrol.* 27 (3), 745–750.
- Liu, J., Chen, J., Zhang, X., Li, Y., Rao, Z., Chen, F., 2015. Holocene East Asian summer monsoon records in northern China and their inconsistency with Chinese stalagmite $\delta^{18}O$ records. *Earth Sci. Rev.* 148, 194–208.
- Liu, X., Sun, Y., Vandenberghe, J., Cheng, P., Zhang, X., Gowan, E.J., Lohmann, G., An, Z., 2020. Centennial- to millennial-scale monsoon changes since the last deglaciation linked to solar activities and North Atlantic cooling. *Clim. Past* 16 (1), 315–324.
- Lowe, D.J., 2011. Tephrochronology and its application: a review. *Quat. Geochronol.* 6 (2), 107–153.
- Lowe, D.J., Shane, P.A.R., Alloway, B.V., Newnham, R.M., 2008. Fingerprints and age models for widespread New Zealand tephra marker beds erupted since 30,000 years ago: a framework for NZ-INTIMATE. *Quat. Sci. Rev.* 27 (1), 95–126.
- Lowe, J., Barton, N., Blockley, S., Ramsey, C.B., Cullen, V.L., Davies, W., Gamble, C., Grant, K., Hardiman, M., Housley, R., Lane, C.S., Lee, S., Lewis, M., MacLeod, A., Menzies, M., Mueller, W., Pollard, M., Price, C., Roberts, A.P., Rohling, E.J., Satow, C., Smith, V.C., Stringer, C.B., Tomlinson, E.L., White, D., Albert, P., Arienzo, I., Barker, G., Boric, S., Carandente, A., Civetta, L., Ferrier, C., Guadelli, J.-L., Karkanas, P., Koumouzelis, M., Mueller, U.C., Orsi, F., Pross, J., Rosi, M., Shalamanov-Korobar, L., Sirakov, N., Tzedakis, P.C., 2012. Volcanic ash layers illuminate the resilience of Neanderthals and early modern humans to natural hazards. *Proc. Natl. Acad. Sci. U.S.A.* 109 (34), 13532–13537.
- Lowe, J.J., Ramsey, C.B., Housley, R.A., Lane, C.S., Tomlinson, E.L., 2015. The RESET project: constructing a European tephra lattice for refined synchronisation of environmental and archaeological events during the last c. 100 ka. *Quat. Sci. Rev.* 118, 1–17.
- Lu, H., Yi, S., Liu, Z., Mason, J.A., Jiang, D., Cheng, J., Stevens, T., Xu, Z., Zhang, E., Jin, L., Zhang, Z., Guo, Z., Wang, Y., Otto-Bliessner, B., 2013. Variation of East Asian monsoon precipitation during the past 21 k.y. and potential CO₂ forcing. *Geology* 41 (9), 1023–1026.
- Machida, H., 1999. The stratigraphy, chronology and distribution of distal marker tephras in and around Japan. *Global Planet. Change* 21 (1), 71–94.
- Machida, H., Arai, F., 1978. Akahoya ash—a Holocene widespread tephra erupted from the Kikai caldera, south Kyushu, Japan. *The Quaternary Research (Daiyonki-Kenkyu)* 17 (3), 143–163 (in Japanese with English abstract).
- Machida, H., Arai, F., 1983. Extensive ash falls in and around the sea of Japan from large late quaternary eruptions. *J. Volcanol. Geoth. Res.* 18 (1–4), 151–164.
- Machida, H., Arai, F., 2003. Atlas of Tephra in and Around Japan, Revised ed. University of Tokyo press, Tokyo, Japan (In Japanese).
- Machida, H., Arai, F., Lee, B.-S., Moriwaki, H., Furuta, T., 1984. Late quaternary tephras in Ulleung-do island, Korea. *J. Geogr.* 93 (1), 1–14 (in Japanese with English abstract).
- Machida, H., Moriwaki, H., Zhao, D.-C., 1990. The recent major eruption of Changbai Volcano and its environmental effects. *Geogr. Rep. Tokyo Metropol. Univ.* (25), 1–20.
- Mackay, H., Hughes, P.D.M., Jensen, B.J.L., Langdon, P.G., Pyne-O'Donnell, S.D.F., Plunkett, G., Froese, D.G., Coulter, S., Gardner, J.E., 2016. A mid to late Holocene cryptotephra framework from eastern North America. *Quat. Sci. Rev.* 132, 101–113.
- Maher, B.A., Thompson, R., 2012. Oxygen isotopes from Chinese caves: records not of monsoon rainfall but of circulation regime. *J. Quat. Sci.* 27 (6), 615–624.
- Mann, M.E., Zhang, Z., Rutherford, S., Bradley, R.S., Hughes, M.K., Shindell, D., Ammann, C., Faluvegi, G., Ni, F., 2009. Global signatures and dynamical origins of the little ice age and medieval climate anomaly. *Science* 326 (5957), 1256–1260.
- Matthews, I.P., Trincardi, F., Lowe, J.J., Bourne, A.J., MacLeod, A., Abbott, P.M., Andersen, N., Asiola, A., Blockley, S.P.E., Lane, C.S., Oh, Y.A., Satow, C.S., Staff, R.A., Wulf, S., 2015. Developing a robust tephrochronological framework for Late Quaternary marine records in the Southern Adriatic Sea: new data from core station SA03-11. *Quat. Sci. Rev.* 118, 84–104.
- McLean, D., Albert, P.G., Nakagawa, T., Staff, R.A., Suzuki, T., Smith, V.C., 2016. Identification of the Changbaishan 'Millennium'(B-Tm) eruption deposit in the Lake Suigetsu (SG06) sedimentary archive, Japan: synchronisation of the hemispheric-wide palaeoclimate archives. *Quat. Sci. Rev.* 150, 301–307.
- McLean, D., Albert, P.G., Nakagawa, T., Suzuki, T., Staff, R.A., Yamada, K., Kitaba, I., Haraguchi, T., Kitagawa, J., Smith, V.C., 2018. Integrating the Holocene tephrostratigraphy for East Asia using a high-resolution cryptotephra study from Lake Suigetsu (SG14 core), central Japan. *Quat. Sci. Rev.* 183, 36–58.
- McLean, D., Albert, P.G., Suzuki, T., Nakagawa, T., Kimura, J.-I., Chang, Q., MacLeod, A., Blockley, S., Staff, R.A., Yamada, K., Kitaba, I., Haraguchi, T., Kitagawa, J., Smith, V.C., 2020. Refining the eruptive history of Ulleungdo and Changbaishan volcanoes (East Asia) over the last 86 kyrs using distal sedimentary records. *J. Volcanol. Geoth. Res.* 389, 106669.
- Miura, K., Hayashi, M., 1991. Quaternary tephra studies in the chugoku and shikoku districts. *The Quaternary Research (Daiyonki-Kenkyu)* 30 (5), 339–351 (in Japanese with English abstract).
- Moriwaki, H., Nakamura, N., Nagasako, T., Lowe, D.J., Sangawa, T., 2016. The role of tephras in developing a high-precision chronostratigraphy for palaeoenvironmental reconstruction and archaeology in southern Kyushu, Japan, since 30,000 cal. BP: an integration. *Quat. Int.* 397, 79–92.
- Nagahashi, Y., Yoshikawa, S., Miyakawa, C., Uchiyama, T., Inouchi, Y., 2004. Stratigraphy and chronology of widespread tephra layers during the past 430ky in the kinki district and the yatsugatake mountains. *The Quaternary Research (Daiyonki-Kenkyu)* 43 (1), 15–35 (in Japanese with English abstract).
- Nakamura, Y., 2016. Stratigraphy, distribution, and petrographic properties of Holocene tephras in Hokkaido, northern Japan. *Quat. Int.* 397, 52–62.
- Nakamura, Y., Hirakawa, K., 2004. Mid-Holocene widespread tephra, komagatake-g (Ko-g) in hokkaido, northern Japan. *The Quaternary Research (Daiyonki-Kenkyu)* 43 (3), 189–200 (in Japanese with English abstract).
- Obrochta, S.P., Yokoyama, Y., Yoshimoto, M., Yamamoto, S., Miyairi, Y., Nagano, G., Nakamura, A., Tsunematsu, K., Lamair, L., Hubert-Ferrari, A., Lougheed, B.C., Hakanishi, A., Yasuda, A., Heyvaert, V.M.A., De Batist, M., Fujiwara, O., 2018. Mt. Fuji Holocene eruption history reconstructed from proximal lake sediments and high-density radiocarbon dating. *Quat. Sci. Rev.* 200, 395–405.
- Okuno, M., Shiihara, M., Torii, M., Nakamura, T., Kim, K.H., Domitsu, H., Moriwaki, H., Oda, M., 2010. AMS radiocarbon dating of Holocene tephra layers on Ulleung Island, South Korea. *Radiocarbon* 52 (3), 1465–1470.
- Okuno, M., Torii, M., Yamada, K., Shinozuka, Y., Danhara, T., Gotanda, K., Yonenobu, H., Yasuda, Y., 2011. Widespread tephras in sediments from lake Ichino-Megata in northern Japan: their description, correlation and significance. *Quat. Int.* 246 (1), 270–277.
- Oppenheimer, C., Wacker, L., Xu, J., Galván, J.D., Stoffel, M., Guillet, S., Corona, C., Sigl, M., Di Cosmo, N., Hajdas, I., Pan, B., Breuer, R., Schneider, L., Esper, J., Fei, J., Hammond, J.O.S., Büntgen, U., 2017. Multi-proxy dating the 'Millennium eruption' of changbaishan to late 946 CE. *Quat. Sci. Rev.* 158, 164–171.
- Pan, B., de Silva, S.L., Xu, J., Chen, Z., Miggins, D.P., Wei, H., 2017. The VEI-7 Millennium eruption, Changbaishan-Tianchi volcano, China/ DPRK: new field, petrological, and chemical constraints on stratigraphy, volcanology, and magma dynamics. *J. Volcanol. Geoth. Res.* 343, 45–59.
- Pan, B., de Silva, S.L., Xu, J., Liu, S., Xu, D., 2020. Late Pleistocene to present day eruptive history of the Changbaishan-Tianchi Volcano, China/ DPRK: new field, geochronological and chemical constraints. *J. Volcanol. Geoth. Res.* 399, 106870.
- Park, M.-H., Kim, I.-S., Shin, J.-B., 2003. Characteristics of the late Quaternary tephra layers in the East/Japan Sea and their new occurrences in western Ulleung Basin sediments. *Mar. Geol.* 202 (3–4), 135–142.
- Park, J., Park, J., Yi, S., Kim, J.C., Lee, E., Choi, J., 2019. Abrupt Holocene climate shifts in coastal East Asia, including the 8.2 ka, 4.2 ka, and 2.8 ka BP events, and societal responses on the Korean peninsula. *Sci. Rep.* 9, 10806.
- Paterne, M., Guichard, F., Labeyrie, J., Gillot, P.Y., Duplessy, J.C., 1986. Tyrrhenian Sea tephrochronology of the oxygen isotope record for the past 60,000 years. *Mar. Geol.* 72 (3), 259–285.
- Paterne, M., Guichard, F., Labeyrie, J., 1988. Explosive activity of the South Italian volcanoes during the past 80,000 years as determined by marine tephrochronology. *J. Volcanol. Geoth. Res.* 34 (3), 153–172.
- Peccerillo, A., Taylor, S., 1976. Geochemistry of Eocene calc-alkaline volcanic rocks from the Kastamonu area, northern Turkey. *Contrib. Mineral. Petrol.* 58 (1), 63–81.
- Ponomareva, V., Portnyagin, M., Pevzner, M., Blaauw, M., Kyle, P., Derkachev, A., 2015. Tephra from andesitic Shiveluch volcano, Kamchatka, NW Pacific: chronology of explosive eruptions and geochemical fingerprinting of volcanic glass. *Int. J. Earth Sci.* 104 (5), 1459–1482.
- Ponomareva, V., Portnyagin, M., Pendea, I.F., Zelenin, E., Bourgeois, J., Pinegina, T., Kozhurin, A., 2017. A full holocene tephrochronology for the kamchatsky peninsula region: applications from Kamchatka to north America. *Quat. Sci. Rev.* 168, 101–122.
- Razjigaeva, N.G., Ganzey, L.A., Ilyashchevskaya, M.S., Makarova, T.R., Kudryavtseva, E.P., Grebennikova, T.A., Panichev, A.M., Arslanov, K., Maksimov, F.E., Petrov, A.Y., Malkov, S.S., 2019. Climatic and human impacts on landscape development of the murav'ev amursky peninsula (Russian south Far East) in the middle/late holocene and historical time. *Quat. Int.* 516, 127–140.

- Razzhigaeva, N.G., Matsumoto, A., Nakagawa, M., 2016. Age, source, and distribution of Holocene tephra in the southern Kurile Islands: evaluation of Holocene eruptive activities in the southern Kurile arc. *Quat. Int.* 397, 63–78.
- Reimer, P.J., Bard, E., Bayliss, A., Beck, J.W., Blackwell, P.G., Bronk Ramsey, C., Buck, C.E., Cheng, H., Edwards, R.L., Friedrich, M., Grootes, P.M., Guilderson, T.P., Haffidason, H., Hajdas, I., Hatté, C., Heaton, T.J., Hoffmann, D.L., Hogg, A.G., Hughen, K.A., Kaiser, K.F., Kromer, B., Manning, S.W., Niu, M., Reimer, R.W., Richards, D.A., Scott, E.M., Southon, J.R., Staff, R.A., Turney, C.S.M., van der Plicht, J., 2013. IntCal13 and Marine13 radiocarbon age calibration curves 0–50,000 Years cal BP. *Radiocarbon* 55 (4), 1869–1887.
- Satow, C., Tomlinson, E.L., Grant, K.M., Albert, P.G., Smith, V.C., Manning, C.J., Ottoloni, L., Wulf, S., Rohling, E.J., Lowe, J.J., Blockley, S.P.E., Menzies, M.A., 2015. A new contribution to the late quaternary tephrostratigraphy of the mediterranean: aegean sea core LC21. *Quat. Sci. Rev.* 117, 96–112.
- Shen, J., Liu, X., Wang, S., Ryo, M., 2005. Palaeoclimatic changes in the Qinghai Lake area during the last 18,000 years. *Quat. Int.* 136 (1), 131–140.
- Shen, J., Wu, X., Zhang, Z., Gong, W., He, T., Xu, X., Dong, H., 2013. Ti content in Huguangyan maar lake sediment as a proxy for monsoon-induced vegetation density in the Holocene. *Geophys. Res. Lett.* 40 (21), 5757–5763.
- Shiwhara, M., Torii, M., Okuno, M., Domitsu, H., Nakamura, T., Kim, K.-H., Moriwaki, H., Oda, M., 2011. Revised stratigraphy of Holocene tephras on Ulleung Island, South Korea, and possible correlatives for the U-Oki tephra. *Quat. Int.* 246 (1), 222–232.
- Shimada, S., 2000. Eruption of the amagi-Kawagodaira volcano and paleoenvironments in the late and latest jomon periods around the izu peninsula. *The Quaternary Research (Daiyonki-kenkyu)* 39 (2), 151–164 (in Japanese with English abstract).
- Siani, G., Sulpizio, R., Paterne, M., Sbrana, A., 2004. Tephrostratigraphy study for the last 18,000 14C years in a deep-sea sediment sequence for the South Adriatic. *Quat. Sci. Rev.* 23 (23), 2485–2500.
- Sigl, M., Winstrup, M., McConnell, J.R., Welten, K.C., Plunkett, G., Ludlow, F., Buntgen, U., Caffee, M., Chellman, N., Dahl-Jensen, D., Fischer, H., Kipfstuhl, S., Kostick, C., Maselli, O.J., Mekhalid, F., Mulvaney, R., Muscheler, R., Pasteris, D.R., Pilcher, J.R., Salzer, M., Schupbach, S., Steffensen, J.P., Vinther, B.M., Woodruff, T.E., 2015. Timing and climate forcing of volcanic eruptions for the past 2,500 years. *Nature* 523 (7562), 543–549.
- Smith, V.C., Mark, D.F., Staff, R.A., Blockley, S.P.E., Ramsey, C.B., Bryant, C.L., Nakagawa, T., Han, K.K., Weh, A., Takemura, K., Danhara, T., 2011. Toward establishing precise 40Ar/39Ar chronologies for Late Pleistocene palaeoclimate archives: an example from the Lake Suigetsu (Japan) sedimentary record. *Quat. Sci. Rev.* 30 (21–22), 2845–2850.
- Smith, V.C., Staff, R.A., Blockley, S.P.E., Bronk Ramsey, C., Nakagawa, T., Mark, D.F., Takemura, K., Danhara, T., 2013. Identification and correlation of visible tephras in the Lake Suigetsu SG06 sedimentary archive, Japan: chronostratigraphic markers for synchronising of east Asian/west Pacific palaeoclimatic records across the last 150 ka. *Quat. Sci. Rev.* 67, 121–137, 0.
- Smith, E.L., Jacobs, Z., Johnsen, R., Ren, M., Fisher, E.C., Oestmo, S., Wilkins, J., Harris, J.A., Karkanas, P., Fitch, S., Ciravolo, A., Keenan, D., Cleghorn, N., Lane, C.S., Matthews, T., Marean, C.W., 2018. Humans thrived in South Africa through the Toba eruption about 74,000 years ago. *Nature* 555, 511.
- Staff, R.A., Bronk Ramsey, C., Bryant, C.L., Brock, F., Payne, R.L., Schlögl, G., Marshall, M.H., Brauer, A., Lamb, H.F., Tarasov, P., Yokoyama, Y., Haraguchi, T., Gotanda, K., Yonenobu, H., Nakagawa, T., 2011. New 14C determinations from lake Suigetsu, Japan: 12,000 to 0 cal BP. *Radiocarbon* 53 (3), 511–528.
- Stebich, M., Rehfeld, K., Schlütz, F., Tarasov, P.E., Liu, J., Mingram, J., 2015. Holocene vegetation and climate dynamics of NE China based on the pollen record from Sihailongwan Maar Lake. *Quat. Sci. Rev.* 124, 275–289.
- Sun, C., Plunkett, G., Liu, J., Zhao, H., Sigl, M., McConnell, J.R., Pilcher, J.R., Vinther, B., Steffensen, J.P., Hall, V., 2014. Ash from Changbaishan Millennium eruption recorded in Greenland ice: implications for determining the eruption's timing and impact. *Geophys. Res. Lett.* 2013GL058642.
- Sun, C., You, H., He, H., Zhang, L., Gao, J., Guo, W., Chen, S., Mao, Q., Liu, Q., Chu, G., Liu, J., 2015. New evidence for the presence of Changbaishan Millennium eruption ash in the Longgang volcanic field, Northeast China. *Gondwana Res.* 28 (1), 52–60.
- Sun, C., Liu, J., You, H., Nemeth, K., 2017. Tephrostratigraphy of Changbaishan volcano, northeast China, since the mid-Holocene. *Quat. Sci. Rev.* 177, 104–119.
- Sun, C., Wang, L., Plunkett, G., You, H., Zhu, Z., Zhang, L., Zhang, B., Chu, G., Liu, J., 2018. Ash from the changbaishan qixiangzhan eruption: a new early holocene marker horizon across East Asia. *J. Geophys. Res.: Solid Earth*, 0(ja).
- Takemura, K., Iwabe, C., Hayashida, A., Danhara, T., Kitagawa, H., Haraguchi, T., Sato, T., Ishikawa, N., 2010. Stratigraphy of marker tephras and sediments during the past 50,000 years from multiple sites in Lake Biwa, Japan. *Quat. Res.* 49 (3), 147–160 (in Japanese with English abstract).
- Tani, S., Kitagawa, H., Hong, W., Park, J.H., Sung, K.S., Park, G., 2013. Age determination of the Kawagodaira volcanic eruption in Japan by 14C wiggle-matching. *Radiocarbon* 55 (2), 748–752.
- Telford, R.J., Heegaard, E., Birks, H.J.B., 2004. All age–depth models are wrong: but how badly? *Quat. Sci. Rev.* 23 (1), 1–5.
- Timms, R.G.O., Matthews, I.P., Lowe, J.J., Palmer, A.P., Weston, D.J., MacLeod, A., Blockley, S.P.E., 2019. Establishing tephrostratigraphic frameworks to aid the study of abrupt climatic and glacial transitions: a case study of the Last Glacial-Interglacial Transition in the British Isles (c. 16–8 ka BP). *Earth Sci. Rev.* 192, 34–64.
- Tomlinson, E.L., Arienzo, I., Civetta, L., Wulf, S., Smith, V.C., Hardiman, M., Lane, C.S., Carandente, A., Orsi, G., Rosi, M., Müller, W., Menzies, M.A., 2012. Geochemistry of the Phlegraean Fields (Italy) proximal sources for major Mediterranean tephras: implications for the dispersal of Plinian and co-ignimbritic components of explosive eruptions. *Geochem. Cosmochim. Acta* 93, 102–128, 0.
- Tsuji, T., Ikeda, M., Furusawa, A., Nakamura, C., Ichikawa, K., Yanagida, M., Nishizaka, N., Ohnishi, K., Ohno, Y., 2018. High resolution record of Quaternary explosive volcanism recorded in fluvio-lacustrine sediments of the Uwa basin, southwest Japan. *Quat. Int.* 471, 278–297.
- Turney, C.S.M., 1998. Extraction of rhyolitic component of Vedde microtephra from minerogenic lake sediments. *J. Paleolimnol.* 19 (2), 199–206.
- van der Bilt, W.G.M., Lane, C.S., Bakke, J., 2017. Ultra-distal Kamchatkan ash on Arctic Svalbard: towards hemispheric cryptotephra correlation. *Quat. Sci. Rev.* 164, 230–235.
- Walker, M., Head, M.J., Lowe, J., Berkelhammer, M., Björck, S., Cheng, H., Cwynar, L.C., Fisher, D., Gkinis, V., Long, A., Newnham, R., Rasmussen, S.O., Weiss, H., 2019. Subdividing the Holocene Series/Epoch: formalization of stages/ages and subseries/subepochs, and designation of GSSPs and auxiliary stratotypes. *J. Quat. Sci.* 34 (3), 173–186.
- Wang, Y., Cheng, H., Edwards, R.L., He, Y., Kong, X., An, Z., Wu, J., Kelly, M.J., Dykoski, C.A., Li, X., 2005. The holocene asian monsoon: links to solar changes and north atlantic climate. *Science* 308 (5723), 854–857.
- Wang, S., Lü, H., Liu, J., Negendank, J.F.W., 2007. The early Holocene optimum inferred from a high-resolution pollen record of Huguangyan Maar Lake in southern China. *Chin. Sci. Bull.* 52 (20), 2829–2836.
- Wang, Y., Cheng, H., Edwards, R.L., Kong, X., Shao, X., Chen, S., Wu, J., Jiang, X., Wang, X., An, Z., 2008. Millennial- and orbital-scale changes in the East Asian monsoon over the past 224,000 years. *Nature* 451, 1090.
- Wang, X., Chu, G., Sheng, M., Zhang, S., Li, J., Chen, Y., Tang, L., Su, Y., Pei, J., Yang, Z., 2016. Millennial-scale Asian summer monsoon variations in South China since the last deglaciation. *Earth Planet Sci. Lett.* 451, 22–30.
- Wen, R., Xiao, J., Fan, J., Zhang, S., Yamagata, H., 2017. Pollen evidence for a mid-Holocene East Asian summer monsoon maximum in northern China. *Quat. Sci. Rev.* 176, 29–35.
- Wu, X., Zhang, Z., Xu, X., Shen, J., 2012. Asian summer monsoon variations during the Holocene revealed by Huguangyan maar lake sediment record. *Palaeogeogr. Palaeoclimatol. Palaeoecol.* 323–325, 13–21.
- Wulf, S., Hardiman, M.J., Staff, R.A., Koutsodendris, A., Appelt, O., Blockley, S.P.E., Lowe, J.J., Manning, C.J., Ottoloni, L., Schmitt, A.K., Smith, V.C., Tomlinson, E.L., Vakhrameeva, P., Knipping, M., Kotthoff, U., Milner, A.M., Müller, U.C., Christianis, K., Kalaitzidis, S., Tzedakis, P.C., Schmiedl, G., Pross, J., 2018. The marine isotope stage 1–5 cryptotephra record of Tenaghi Philippon, Greece: towards a detailed tephrostratigraphic framework for the Eastern Mediterranean region. *Quat. Sci. Rev.* 186, 236–262.
- Xiao, J., Xu, Q., Nakamura, T., Yang, X., Liang, W., Inouchi, Y., 2004. Holocene vegetation variation in the Daihai Lake region of north-central China: a direct indication of the Asian monsoon climatic history. *Quat. Sci. Rev.* 23 (14), 1669–1679.
- Yamamoto, T., Ito, J.-i., Nakagawa, M., Hasegawa, T., Kishimoto, H., 2010. 14 C ages for the ejecta from Kutcharo and Mashu calderas, eastern Hokkaido, Japan. *Bull. Geol. Surv. Jpn.* 61 (5–6), 161–170 (in Japanese with English abstract).
- Yoshimoto, M., Amma-Miyasaka, M., Takahashi, R., Nakagawa, M., Yoshida, K., 2008. Reevaluation of the pre-1640 AD eruptive history of Hokkaido-Komagatake volcano, northern Japan. *J. Geol. Soc. Jpn.* 114, 336–347 (in Japanese with English abstract).
- Zanchetta, G., Sulpizio, R., Roberts, N., Cioni, R., Eastwood, W.J., Siani, G., Caron, B., Paterne, M., Santacrose, R., 2011. Tephrostratigraphy, chronology and climatic events of the Mediterranean basin during the Holocene: an overview. *Holocene* 21 (1), 33–52.
- Zanchetta, G., Bini, M., Di Vito, M.A., Sulpizio, R., Sadori, L., 2019. Tephrostratigraphy of paleoclimatic archives in central mediterranean during the bronze age. *Quat. Int.* 499, 186–194.
- Zheng, Y., Pancost, R.D., Naafs, B.D.A., Li, Q., Liu, Z., Yang, H., 2018. Transition from a warm and dry to a cold and wet climate in NE China across the Holocene. *Earth Planet Sci. Lett.* 493, 36–46.
- Zhou, W., Xie, S., Meyers, P.A., Zheng, Y., 2005. Reconstruction of late glacial and Holocene climate evolution in southern China from geolipids and pollen in the Dingnai peat sequence. *Org. Geochem.* 36 (9), 1272–1284.
- Zhou, X., Sun, L., Zhan, T., Huang, W., Zhou, X., Hao, Q., Wang, Y., He, X., Zhao, C., Zhang, J., Qiao, Y., Ge, J., Yan, P., Yan, Q., Shao, D., Chu, Z., Yang, W., Smol, J.P., 2016. Time-transgressive onset of the holocene optimum in the east asian monsoon region. *Earth Planet Sci. Lett.* 456, 39–46.
- Öba, Y., Katsui, Y., Kurasawa, H., Ikeda, Y., Uda, T., 1983. Petrology of historic rhyolite and dacite from Uzu volcano, North Japan. *J. Fac. Sci. Hokkaido Univ. - Ser. 4 Geol. Mineral.* 20 (4), 275–290.